Global and Planetary Change 139 (2016) 128–140

Contents lists available at ScienceDirect

Global and Planetary Change

journal homepage: www.elsevier.com/locate/gloplacha

# Rapid early Holocene sea-level rise in Prydz Bay, East Antarctica

Dominic A. Hodgson [a,b,*], Pippa L. Whitehouse [b], Gijs De Cort [c,d,e,1], Sonja Berg [f], Elie Verleyen [c], Ines Tavernier [c], Stephen J. Roberts [a], Wim Vyverman [c], Koen Sabbe [c], Philip O'Brien [g]

[a] British Antarctic Survey, Natural Environment Research Council, High Cross, Madingley Road, Cambridge CB3 0ET, UK
[b] Department of Geography, Durham University, South Road, Durham DH1 3LE, UK
[c] Laboratory for Protistology and Aquatic Ecology, Biology Department, Ghent University, Krijgslaan 281–S8, 9000 Ghent, Belgium
[d] Limnology Unit, Biology Department, Ghent University, K.L. Ledeganckstraat 35, 9000 Ghent, Belgium
[e] Department of Earth Sciences, Royal Museum for Central Africa, Leuvensesteenweg 13, 3080 Tervuren, Belgium
[f] Institute of Geology and Mineralogy, University of Cologne, Zuelpicher Strasse 49a, 50674 Cologne, Germany
[g] Department of Environmental Sciences, Macquarie University, NSW 2109, Australia

ARTICLE INFO

*Article history:*
Received 12 June 2015
Received in revised form 14 December 2015
Accepted 29 December 2015
Available online 15 January 2016

*Keywords:*
East Antarctic Ice Sheet
Deglaciation
Sea level rise
Prydz Bay
Lambert Glacier

ABSTRACT

Prydz Bay is one of the largest embayments on the East Antarctic coast and it is the discharge point for approximately 16% of the East Antarctic Ice Sheet. Geological constraints on the regional ice sheet history include evidence of past relative sea-level change at three sites; the Vestfold Hills, Rauer Islands and Larsemann Hills. In this paper we compile updated regional relative sea-level data from these sites. We compare these with a suite of relative sea-level predictions derived from glacial isostatic adjustment models and discuss the significance of departures between the models and the field evidence. The compiled geological data extend the relative sea-level curve for this region to 11,258 cal yr BP and include new constraints based on abandoned penguin colonies, new isolation basin data in the Vestfold Hills, validation of a submarine relative sea-level constraint in the Rauer Islands and recalibrated radiocarbon ages at all sites dating from 12,728 cal yr BP. The field data show rapid increases in rates of relative sea level rise of 12–48 mm/yr between 10,473 (or 9678) and 9411 cal yr BP in the Vestfold Hills and of 8.8 mm/yr between 8882 and 8563 cal yr BP in the Larsemann Hills. The relative sea-level high stands of ≥8.8 m from 9411 to after 7564 cal yr BP (Vestfold Hills) and ≥8 m at 8563 and 7066 cal yr BP (Larsemann Hills) are over-predicted by some of the glacial isostatic adjustment models considered here, suggesting that assumptions relating to the magnitude and timing of regional ice loss since the Last Glacial Maximum may need revising. In the Vestfold Hills and Rauer Islands the final deglacial sea-level rise was almost exactly cancelled out by local rebound between 9411 and 5967 cal yr BP and this was followed by a near exponential decay in relative sea-level. In the Larsemann Hills the sea-level data suggest that the rate of ice retreat in this region was not uniform throughout the Holocene. Swath bathymetric surveys of the benthic seafloor topography show the presence of multiple offshore basins. These are a priority for further study as those that remained free of grounded ice should provide precise constraints on relative sea-level rise and ice sheet history during the most rapid phases of the last major deglaciation.



## 1. Introduction

The Antarctic Ice Sheet represents the largest potential source of future sea-level rise but the rate at which this reservoir will be depleted is not easily quantifiable (Church et al., 2013). Model inter-comparison exercises have shown that the ice sheet is particularly sensitive to basal melting beneath floating ice shelves, to basal sliding (Bindschadler et al., 2013) and, in areas of marine based ice, to sea level changes. However, uncertainties remain with regard to the timing and magnitude of the ice sheet response to potential future climate scenarios, and the 'likely' magnitude of sea-level rise during the next century due to dynamic ice discharge from Antarctica is considered by the IPCC to lie in the range of -20 to + 185 mm (Church et al., 2013).

One way of reducing the wide range of such estimates is to develop detailed knowledge of the glacial loading history; this provides a template for future rates of change, and is a necessary requirement for calculating present-day rates of ice mass change from satellite gravity observations (Wahr et al., 2000). Regional ice loading history can be inferred from changes in relative sea-level (RSL) and GPS bedrock uplift data, while point observations of past ice thickness and extent can be derived from ice cores and exposure dating of nunataks. RSL is the

* Corresponding author at: British Antarctic Survey, Natural Environment Research Council, High Cross, Madingley Road, Cambridge CB3 0ET, UK.
*E-mail address:* daho@bas.ac.uk (D.A. Hodgson).
[1] Present affiliation.

http://dx.doi.org/10.1016/j.gloplacha.2015.12.020

relative vertical displacement between the sea surface and the land over a period of time. It is influenced by changes in ocean volume (eustatic changes in sea level) and deformation of the geoid and solid Earth (isostatic changes) caused by changes in the mass of overlying ice and ocean loads (Farrell and Clark, 1976). Reconstructions of RSL are critical for constraining regional ice-loading histories, and hence the gravitational signal associated with the ongoing solid Earth response to past ice load changes, a process known as Glacial Isostatic Adjustment (GIA). Knowledge of the GIA signal is necessary for improving the accuracy of satellite gravity based estimates of ice mass change because it enables the separation of *ice* mass change from *total* mass change via the subtraction of the GIA signal.

RSL can be determined in two main ways: by studying raised marine landforms (beaches, deltas etc.), and by studying isolation basins (Roberts et al., 2011). In the former case, raised marine features are sampled for organic material or calcified fossils such as shells, seal skin, penguin remains, or whalebone that can provide an age estimate or constraining date for the minimum age of the beach. In the case of isolation basins, cores are taken from lakes near sea level along the coastal margin. Prior to deglaciation, and depending on their altitude, these lakes may have been former marine inlets or basins. Following deglaciation, as crustal rebound outpaced sea-level rise, they became isolated and transformed into freshwater, or brackish, lakes. The sediments in many coastal Antarctic lakes accurately record this transition (Roberts et al., 2011; Verleyen et al., 2005; Watcham et al., 2011), which can be dated to determine when the basin sill was at sea level. This approach can be used for lakes at different altitudes, allowing a reconstruction of RSL changes through time that is more precise than can be achieved using the raised beach approach.

The Amery Ice Shelf (Fig. 1) is one of the main sources of ice loss along the East Antarctic coastline, discharging ice from the Lambert Glacier and other glaciers into Prydz Bay. As a result there have been several studies of RSL changes at ice-free areas in this region including the Vestfold Hills (Zwartz et al., 1998), Larsemann Hills (Hodgson et al., 2009; Verleyen et al., 2004a, 2005) and Rauer Islands (Berg et al., 2010). This network of sites potentially enables an evaluation of local versus regional changes in ice volume and a robust assessment of regional ice mass change through the Holocene.

The aims of this paper are to consolidate and validate existing and new RSL evidence from the Prydz Bay region and compare the resulting sea-level curves with predictions from a suite of GIA models. We discuss the significance of departures between field evidence and model predictions and identify priorities for future research.

### 1.1. Site description

Prydz Bay occupies the East Antarctic coastline between 60 and 80° E and 65 and 70° S (Fig. 1). It marks the end of the major glacial trough eroded by the Lambert-Amery system that extends 1000 km into the continental interior and which is eroded to 2560 m below sea level (Damm, 2007). Ice from as far inland as Dome Argus and Dome Fuji converges into outlet glaciers such as the Lambert, Mellor and Charybdis glaciers that flow through the Prince Charles Mountains in Mac. Robertson Land. These glaciers terminate in the Lambert Glacier/Amery Ice Shelf system; draining approximately 16% of the East Antarctic Ice Sheet and discharging icebergs and meltwater into Prydz Bay (Mackintosh et al., 2014).

## 2. Methods

There are a number of ice-free regions along the coast of Prydz Bay, including the Vestfold Hills, Rauer Islands and Larsemann Hills, which contain evidence of past sea-level changes, including raised beaches, isolation basins and stranded marine deposits from which RSL curves can be derived (Zwartz et al., 1998). This compilation of RSL data from the Prydz Bay region includes previously published data from the Larsemann Hills (Verleyen et al., 2005) and Vestfold Hills (Adamson and Pickard, 1983; Bird et al., 1991; Coolen et al., 2004; Pickard, 1985; Pickard and Adamson, 1983; Pickard and Seppelt, 1984; Zhang and Peterson, 1984; Zwartz et al., 1998) which have been re-evaluated in terms of maximum and minimum sea-level constraints; all radiocarbon dates have been recalibrated (Table 1). To these we have added new constraints based on the location, altitude and age of abandoned penguin colonies in the Vestfold Hills (Huang et al., 2011; Huang et al., 2009a, 2009b) and we have carried out a detailed study to validate a potential submarine RSL constraint in the Rauer Islands, which was previously identified in a marine sediment core by Berg et al. (2010). This last constraint is important as it is the only one from the early Holocene, it predates the local RSL maximum, and it constrains the rising limb of the RSL curve. In the Larsemann Hills there has been no additional geological data since Verleyen et al. (2005) with the exception of one isolation basin constraint in Marine Isotope Stage 3 (MIS3) (Hodgson et al., 2009) and 5 mumiyo (Snow Petrel pro-ventricular stomach oil deposits) radiocarbon dates from nesting sites at altitudes of 75–100 m (Kiernan et al., 2009).

Validation of the RSL constraint in the Rauer Islands involved high resolution diatom analysis and radiocarbon dating of the 1087–900 cm section of the Co1011 sediment core recovered by Berg et al. (2010) offshore from Flag Island. Sixteen diatom samples were analysed at 2–12 cm intervals to identify marine-freshwater transitions following methods described in Watcham et al. (2011) and Roberts et al. (2011) with taxonomy based on Roberts and McMinn (1999); Sabbe et al. (2003); Cremer et al. (2003) and data assembled for Verleyen et al. (2003). Total diatom abundances were determined from microspheres following Battarbee and Kneen (1982). Tilia (Grimm, 1991) and TGView 2.0.2 software (Grimm, 2004) were used to generate stratigraphic plots, and CONISS (Grimm, 1987) was used to provide a constrained cluster analysis. Ordinations of log-transformed species data were carried out in CANOCO 4.5 for Windows (ter Braak and Smilauer, 2002). First a detrended correspondence analysis (DCA) was used to calculate the length of gradient of the dataset (2.953) and this was followed by correspondence analysis (CA).

A chronology for the core section was derived from seven AMS radiocarbon dates calibrated in Calib 7.1 using the southern hemisphere SHCal13.14c calibration curve (Hogg et al., 2013) for freshwater sediments and the Marine13.14c calibration curve (Reimer et al., 2013) for marine sediments. Dates from marine sediments were corrected for the local marine carbon reservoir effect of 900 years, based on a surface sediment age correction (Berg et al., 2010). At the lacustrine-marine transition, a composite reservoir effect of 665 years was applied based on the relative abundances of marine and freshwater diatom species at this depth (73.9%, see results). To derive interpolated ages a smooth spline age-depth model was applied with a smoothing factor of 0.2 and 10,000 iterations weighted by calibrated probabilities at 95% confidence ranges and a resolution of 1 year steps using CLAM software in R (Blaauw, 2010).

Radiocarbon age data are reported as conventional radiocarbon years BP ($^{14}$C yr BP), as 2-σ (95.4%) calibrated age ranges and median calibrated ages (cal yr BP, relative to AD 1950). Where a reservoir correction is included in the calibration, ages are reported as corrected ages (corrected yr BP). Where ages are calculated between two calibrated radiocarbon dates, ages are reported as 'interpolated cal yr BP'. The caption to Table 1 provides further details.

### 2.1. Deriving a RSL curve from the geological constraints

Data associated with the termination of lacustrine-to-marine transitions are plotted on the RSL curve (because sea level has fully inundated the site by this time) whereas the data associated with the termination of marine-to-lacustrine transitions are plotted on or just above the RSL curve (as sea level falls). Dated marine deposits such as in situ shells of the bivalve *Laternula elliptica*, which typically live below the intertidal zone, are plotted below the relative sea-level curve. Conversely radiocarbon-dated abandoned penguin nest sites provide upper constraints for sea level and are plotted above the curve. In the Vestfold

Hills the exact transitions in the isolation basin sediment cores are less-well constrained by multiproxy datasets, compared with the Larsemann Hills and Rauer Islands data, so the curve is plotted through the first published lacustrine age. In most cases multiple core samples were analysed across transitions thereby ruling out transient incursions of marine water from storm, or iceberg calving events.

Measurements of the altitudes of the sills of isolation basins were cross-referenced against geodetic data (where available). Where published data were referenced to mean sea level as opposed to peak tidal range, the marine-to-lacustrine and lacustrine-to-marine transitions have a vertical error of 0.87 m (half the tidal range) (Zwartz et al., 1998). The sill height of the Flag Island depression is reported in the RV Polarstern expedition ANT XXIII/9 Cruise Report as −4 m. This was determined using an echo sounder from the coring platform at 11 am on 10th March 2007. The nearest tide gauge (Davis Station) recorded 7.39 m during the survey which is 40 cm below the maximum tide for that month. We therefore assign an error of +/−40 cm to the depth measurement. Future differential GPS surveys should be a priority to further reduce these vertical errors.

### 2.2. GIA modelling

The regional RSL data compilations are compared with published model predictions of RSL associated with four deglacial models for Antarctica, each of which has previously been used to predict RSL change in Prydz Bay. These models are (i) the model of Briggs et al. (2013, 2014; hereafter known as BPT14), (ii) the ICE-6G_C (VM5a) model (Argus et al., 2014; Peltier et al., 2015), (iii) the model of Gomez et al. (2013, hereafter known as GPM13) and (iv) the W12 model (Whitehouse et al., 2012a). The BPT14 and ICE-6G_C (VM5a) models are global deglacial models, while the GPM13 and W12 models adopt the ICE-5G model (Peltier, 2004) outside Antarctica. In all cases the results shown here are directly reproduced from the original publications.

In order to produce the previously published results, each deglaciation model was combined with a model of Earth rheology in order to calculate the evolution of RSL through time. The BPT14 and ICE-6G_C (VM5a) models used the VM5a Earth model (Peltier and Drummond, 2008); the GPM13 model used an Earth model characterised by a lithospheric thickness of 100 km, an upper mantle viscosity of $5 \times 10^{20}$ Pa s, and a lower mantle viscosity of $5 \times 10^{21}$ Pa s; while the results for the W12 model were produced using the 'optimum' Earth model of Whitehouse et al. (2012b), which comprises a 120 km-thick lithosphere, an upper mantle viscosity of $10^{21}$ Pa s, and a lower mantle viscosity of $10^{22}$ Pa s. All models use a spherical harmonic approach, and calculate solutions up to degree and order 256, except the GPM13 model, which uses degree and order 512. The resolution used can affect model results.

## 3. Results

### 3.1. Geological constraints on RSL

The compiled geological data extend the original sea-level curve for this region (Zwartz et al., 1998) from 7564 cal yr BP to 11,258 cal yr BP (Table 1). Notable results presented in Table 1 include a new age for the inundation of Ace Lake at 9411 cal yr BP (Coolen et al., 2004), and radiocarbon dates on a series of penguin fossils at abandoned penguin nesting sites at 7 m and 32 m respectively on Zolotov and Gardner Islands (Huang et al., 2009a, 2009b, 2011) constraining the sea level maximum. However, we begin by presenting new data from the Rauer Islands.

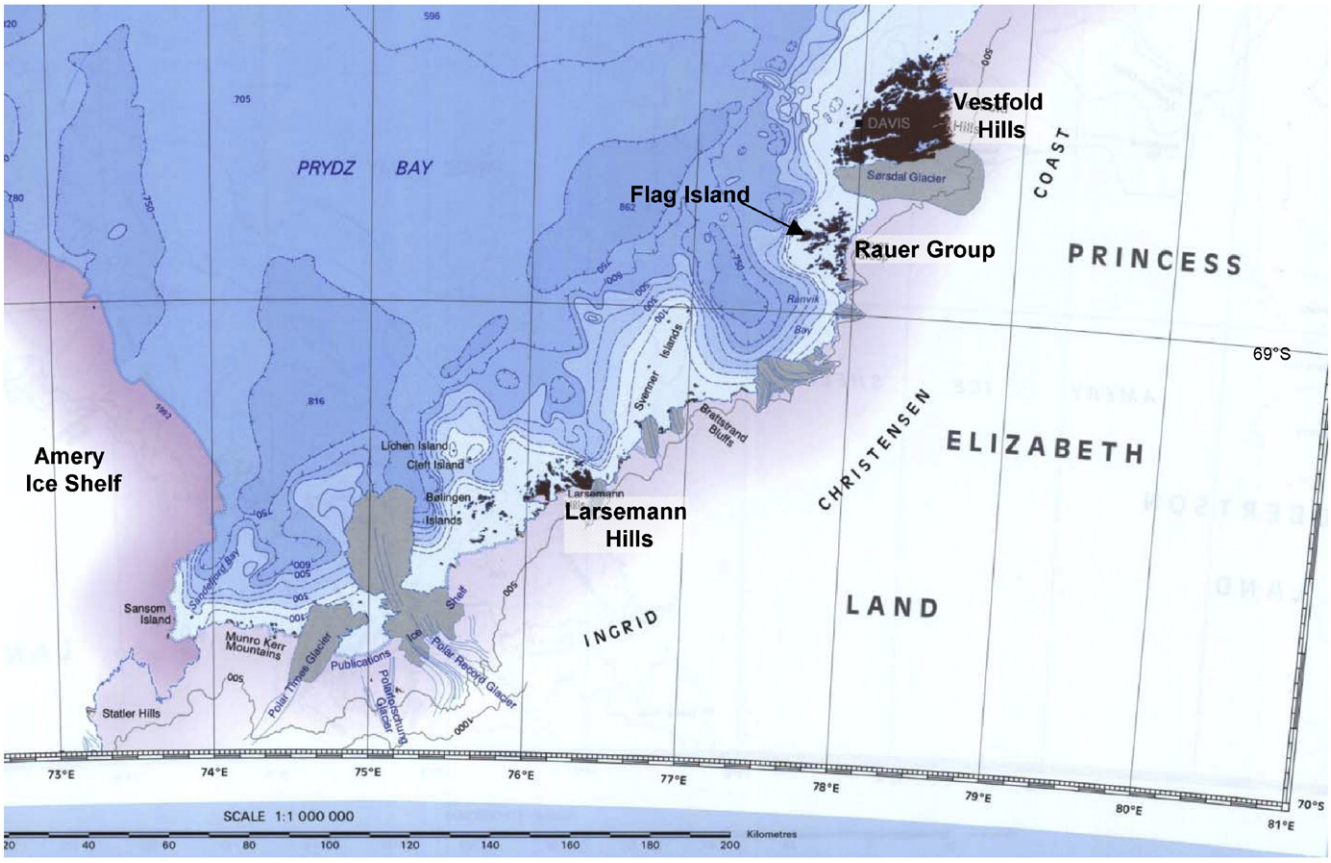


**Fig. 1.** Location map. Extracted from the Scientific Committee for Antarctic Research (SCAR) Map Catalogue, Prydz Bay, Map 7, 1997, Scale 1:1 000 000, Australian Antarctic Data Centre.

**Table 1**

Radiocarbon ages used to constrain RSL in the Prydz Bay region. Dates were calibrated in Calib 7.1 using the Marine13.14c calibration curve (Marine) (Reimer et al. 2013) for marine sediments, the southern hemisphere SHCal13.14c (SH) calibration curve (Hogg et al., 2013) for freshwater sediments, and mixed SH terrestrial and marine calibration datasets (Mixed). Radiocarbon age data are reported as conventional radiocarbon years BP ($^{14}$C yr BP) and as 2-σ (95.4%) calibrated age ranges, median calibrated ages (cal yr BP relative to AD 1950). The radiocarbon reservoir effect for marine sediments in the Rauer Islands, Larsemann Hills and Vestfold Hills is based on a surface age correction of 900 years (Berg et al., 2010a) with a Delta R of 500 (based on the local core top reservoir correction of 900 minus the global marine reservoir of 400). In the Flag Island depression core (CO1101) the ratio of marine to lacustrine diatom species at a depth of 1067 cm equalled 0.739 and was used to calculate the mixed reservoir effect for this sample. An additional age depth model was constructed using the SHCal04.14C calibration curve in CLAM (Blaauw, 2010) to provide interpolated ages at various depths during the transition. To permit clear cross-referencing between the table and text, dates are not rounded. *Where age ranges are presented we cite the full age ranges in the model.

The calibrated bulk radiocarbon age of 12,728 cal yr BP at 1089–1087 cm depth in the analysed section of the Rauer Islands core (Table 1, Fig. 2), based on the best fit in the age-depth model, is slightly older than the two moss macrofossils at the same depth (Table 1). We use the younger ages in the age-depth model because typically in Antarctica terrestrial and lacustrine macrofossils provide more reliable ages than bulk samples which can be contaminated by old meltwater containing dissolved carbon depleted in $^{14}$C (Hall and Henderson, 2001), especially for samples at the glacial/deglacial transition.

For the upper lying lacustrine sample at 1078 cm, no lake reservoir correction was applied. This is based on the hypothesis that the lake was mainly fed by precipitation and melting of snowbanks in the catchment at that time, as the area was under the influence of the relatively wet Early Holocene climatic optimum that has been inferred for the whole of East Antarctica (Verleyen et al., 2011). Furthermore, TS levels (Fig. 4) suggest that the sediment was deposited under a well-mixed water column and seasonally ice-free conditions, indicating that the lake water was in equilibrium with the atmosphere at this time.

| Lake/Location | Lat/Long | Core depth (cm) | Height (m asl) | Material dated | Lab code | Conv. 14C age | Error | Reservoir correction | Delta R | % marine | Model | Recal. age range (lower) | Recal. age range (upper) | Relative area under probability function | Median probability | Original cited age* | Comment | Reference |
|---|---|---|---|---|---|---|---|---|---|---|---|---|---|---|---|---|---|---|
| *Rauer Islands isolation basin* | | | | | | | | | | | | | | | | | | |
| Flag Is. depression | 68°49′35″, 77°46′24″ | 902–900 | −4 ± 0.4 | Bulk marine sed | KIA37746 | 8530 | 45 | 900 | 500 | 100 | Marine | 8386 | 8582 | 1 | 8483 | | Marine sediments | Berg et al., 2010 |
| Flag Is. depression | 68°49′35″, 77°46′24″ | 1048–1047 | −4 ± 0.4 | Bulk marine sed | BETA305736 | 9220 | 50 | 900 | 500 | 100 | Marine | 9269 | 9490 | 1 | 9396 | | Marine sediments | This Paper |
| Flag Is. depression | 68°49′35″, 77°46′24″ | 1050 | −4 ± 0.4 | Interpolated age | | | | | | | | | | | 9678 | | L-M transition complete | This Paper |
| Flag Is. depression | 68°49′35″, 77°46′24″ | 1067–1065 | −4 ± 0.4 | Bulk transition sed | BETA305737 | 9020 | 40 | 665 | 265 | 74 | Mixed | 9470 | 9651 | 1 | 9539 | | L-M transition | This Paper |
| Flag Is. depression | 68°49′35″, 77°46′24″ | 1073 | −4 ± 0.4 | Interpolated age | | | | | | | | | | | 10,473 | | L-M transition onset | This Paper |
| Flag Is. depression | 68°49′35″, 77°46′24″ | 1079–1077 | −4 ± 0.4 | Bulk lacustrine sed | BETA305738 | 9610 | 50 | 0 | 0 | 0 | SH | 10,714 | 11,128 | 1 | 10,929 | | Lacustrine sediments | This Paper |
| Flag Is. depression | 68°49′35″, 77°46′24″ | 1089–1087 | −4 ± 0.4 | Bulk lacustrine sed | BETA305739 | 10,880 | 50 | 0 | 0 | 0 | SH | 12,681 | 12,804 | 1 | 12,728 | | Lacustrine sediments | This Paper |
| Flag Is. depression | 68°49′35″, 77°46′24″ | 1089–1087 | −4 ± 0.4 | Plant macrofossil | BETA305951 | 9640 | 50 | 0 | 0 | 0 | SH | 10,749 | 11,161 | 1 | 10,941 | 11,184 | Lacustrine sediments | This Paper |
| Flag Is. depression | 68°49′35″, 77°46′24″ | 1089–1087 | −4 ± 0.4 | Plant macrofossil | KIA37748 | 9890 | 60 | 0 | 0 | 0 | SH | 11,158 | 11,407 | 0.977 | 11,258 | 11,184 | Lacustrine sediments | Berg et al., 2010 |
| *Larsemann Hills isolation basins* | | | | | | | | | | | | | | | | | | |
| Pup Lagoon | 69°23′57″, 76° 05′26″ | 150 | 4 ± 0.5 | Organic fraction | AA-35,751 | 2150 | 45 | 0 | 0 | 0 | SH | 1995 | 2184 | 0.871 | 2092 | 2002–2307 | M-L transition | Verleyen et al., 2005 |
| Heart Lake | 69°22′34″, 76° 22′55″ | 20 | 5 ± 0.5 | Cyanobacteria | AA-35,736 | 2620 | 45 | 0 | 0 | 0 | SH | 2676 | 2781 | 0.561 | 2703 | 2509–2847 | M-L transition | Verleyen et al., 2005 |
| Heart Lake | 69°22′34″, 76° 22′55″ | 245 | 5 ± 0.5 | Organic fraction | AA-35,739 | 8070 | 75 | 0 | 0 | 0 | SH | 8636 | 9094 | 0.986 | 8882 | 9260–8650 | L-M transition | Verleyen et al., 2005 |
| Heart Lake | 69°22′34″, 76° 22′55″ | 275 | 5 ± 0.5 | Organic fraction | AA-41,164 | 8508 | 59 | 0 | 0 | 0 | SH | 9397 | 9546 | 0.939 | 9481 | 9420–9560 | Lacustrine sediments | Verleyen et al., 2005 |
| Heart Lake | 69°22′34″, 76° 22′55″ | 360 | 5 ± 0.5 | Organic plus silt | AA-41,633 | 10,314 | 65 | 900 | 500 | 100 | Marine | 10,566 | 10,970 | 1 | 10,740 | 10,360–9910 | Marine sediments | Verleyen et al., 2005 |
| Kirisjes Pond | 69°22′59″, 76° 07′27″ | 86 | 8 ± 0.5 | Cyanobacteria | AA-35,744 | 6205 | 50 | 0 | 0 | 0 | SH | 6903 | 7179 | 0.972 | 7066 | 6950–7250 | M-L transition | Verleyen et al., 2005 |
| Kirisjes Pond | 69°22′59″, 76° 07′27″ | 110 | 8 ± 0.5 | Organic fraction | AA-35,745 | 7825 | 70 | 900 | 500 | 100 | SH | 8404 | 8775 | 0.996 | 8563 | 7270–7510 | L-M transition | Verleyen et al., 2005 |
| Kirisjes Pond | 69°22′59″, 76° 07′27″ | 124 | 8 ± 0.5 | Cyanobacteria | AA-35,746 | 8545 | 60 | 0 | 0 | 0 | SH | 9402 | 9561 | 0.986 | 9501 | | Lacustrine sediments | |
| Kirisjes Pond | 69°22′59″, 76° 07′27″ | 138 | 8 ± 0.5 | Cyano., org, silt | AA-35,747 | 10,400 | 65 | 0 | 0 | 0 | SH | 11,952 | 12,430 | 1 | 12,210 | | Lacustrine sediments | |
| *Vestfold Hills isolation basins* | | | | | | | | | | | | | | | | | | |

(continued on next page)

**Table 1** (*continued*)

| Lake/Location | Lat/Long | Core depth (cm) | Height (m asl) | Material dated | Lab code | Conv. 14C age | Error | Reservoir correction | Delta R | % marine | Model | Recal. age range (lower) | Recal. age range (upper) | Relative area under probability function | Median probability | Original cited age* | Comment | Reference |
|---|---|---|---|---|---|---|---|---|---|---|---|---|---|---|---|---|---|---|
| Organic Lake | 68°27′23″, 78° 11′22″ | 30–47 | 3.5 | Bulk organic sed | ANU-6214 | 2440 | 90 | 0 | 0 | 0 | SH | 2304 | 2741 | 0.982 | 2482 | | Lacustrine, 7–24 cm above M-L transition | Bird et al., 1991 |
| Organic Lake | 68°27′23″, 78° 11′22″ | 54 | 3.5 | Interpolated age | | | | | | | | | | | | 2828 | M-L transition | |
| Organic Lake | 68°27′23″, 78° 11′22″ | 47–60 | 3.5 | Bulk organic sed | ANU-6407 | 4770 | 180 | 900 | 500 | 50 | Mixed SH | 4424 | 5329 | 0.984 | 4924 | | Marine, −6 to 6 cm spanning M-L transition | Bird et al., 1991 |
| Highway Lake | 68°27′49″, 78° 13′26″ | 179–209 | 7.7 | Bulk organic sed | ANU-6213 | 4120 | 70 | 0 | 0 | 0 | SH | 4423 | 4821 | 1 | 4598 | | Lacustrine, 3–30 cm above M-L transition | Bird et al., 1991 |
| Highway Lake | 68°27′49″, 78° 13′26″ | 212 | 7.7 | Interpolated age | | | | | | | | | | | | 5928 | M-L transition | |
| Highway Lake | 68°27′49″, 78° 13′26″ | 209–249 | 7.7 | Bulk organic sed | ANU-6406 | 6060 | 150 | 900 | 500 | 7 | Mixed SH | 6440 | 7172 | 1 | 6806 | | minus 3–40 cm spanning M-L transition | Bird et al., 1991 |
| Watts Lake | 68°36′10″, 78° 13′07″ | 13–14 | 4.3 | Bulk organic sed | AMS-334 | 3250 | 340 | 0 | 0 | 0 | SH | 2702 | 4411 | 0.997 | 3436 | | 0–1 cm above M-L transition | Zwartz et al., 1998 |
| Watts Lake | 68°36′10″, 78° 13′07″ | 14 | 4.3 | Interpolated age | | | | | | | | | | | | 4195 | M-L transition | |
| Lake Druzhby | 68°35′29″, 78° 16′20″ | 25–30 | 8 | Bulk organic sed | ANU-8147 | 5240 | 200 | 0 | 0 | 0 | SH | 5583 | 6400 | 0.998 | 5967 | | 0–5 cm above M-L transition | Zwartz et al., 1998 |
| Lake Druzhby | 68°35′29″, 78° 16′20″ | 30 | 8 | Interpolated age | | | | | | | | | | | | 6749 | M-L transition | |
| Anderson Lake | 68°36′28″, 78° 10′19″ | 38–43 | 8.4 | Bulk organic sed | ANU-8446 | 6730 | 200 | 0 | 0 | 0 | SH | 7240 | 7943 | 0.988 | 7564 | | 0–5 cm above M-L transition | Zwartz et al., 1998 |
| Anderson Lake | 68°36′28″, 78° 10′19″ | 43 | 8.4 | Interpolated age | | | | | | | | | | | | | M-L transition | |
| Anderson Lake | 68°36′28″, 78° 10′19″ | 103 | 8.4 | Interpolated age | | | | | | | | | | | | 5891 | L-M transition | |
| Anderson Lake | 68°36′28″, 78° 10′19″ | 103–107 | 8.4 | Bulk organic sed | ANU-8349 | 7110 | 210 | 0 | 0 | 0 | SH | 7565 | 8330 | 0.997 | 7899 | | Marine, 0–4 cm below L-M transition | Zwartz et al., 1998 |
| Ace Lake | 68°28′17″, 78° 11′16″ | 20–35 | 8.8 | Bulk organic sed | ANU-6414 | 5310 | 90 | 0 | 0 | 0 | SH | 5891 | 6281 | 0.988 | 6059 | 7676 | Lacustrine, 0–15 cm above M-L transition | Zwartz et al., 1998 |
| Ace Lake | 68°28′17″, 78° 11′16″ | 35 | 8.8 | Interpolated age | | | | | | | | | | | | | M-L transition | |
| Ace Lake | 68°28′17″, 78° 11′16″ | 130 | 8.8 | Interpolated age | | | | | | | | | | | | | L-M transition | |
| Ace Lake | 68°28′17″, 78° 11′16″ | 135–140 | 8.8 | Bulk organic sed | ANU-8263 | 6740 | 230 | 0 | 0 | 0 | SH | 7156 | 8013 | 0.996 | 7572 | | Lacustrine, 5–10 cm below L-M transition | Zwartz et al., 1998 |
| Ace Lake | 68°28′17″, 78° 11′16″ | 65–67 | 8.8 | Bulk organic sed | | 5200 | 50 | 0 | 0 | 0 | SH | 5744 | 6005 | 0.987 | 5915 | 5560 ± 100 | Lacustrine, 12–14 cm above M-L transition | Coolen et al., 2004 |
| Ace Lake | 68°28′17″, 78° 11′16″ | 79 | 8.8 | Interpolated age | | | | | | | | | | | | | M-L interpolated age | |
| Ace Lake | 68°28′17″, 78° 11′16″ | 89–91 | 8.8 | Bulk organic sed | | 5620 | 50 | 900 | 500 | 100 | Marine | 5331 | 5579 | 1 | 5488 | 5900 ± 115 | Marine, 10–21 cm below M-L transition | Coolen et al., 2004 |
| Ace Lake | 68°28′17″, 78° 11′16″ | 133–135 | 8.8 | Bulk organic sed | | 8830 | 50 | 900 | 500 | 50 | Mixed SH | 9280 | 9505 | 1 | 9411 | 9400 ± 120 | L-M transition | Coolen et al., 2004 |
| *Vestfold Hills raised beaches* | | | | | | | | | | | | | | | | | | |
| Mud Lake | 68°38′58″, 77° 57′19″ | | 3 | shells | ZDL66 | 3325 | 103 | 900 | 500 | 100 | Marine | 2313 | 2775 | 1 | 2561 | 2000 | Lower constraint on sea level | Zhang and Peterson, 1984 |
| Mud Lake | 68°38′58″, 77° 57′19″ | | 3 | shells | ZDL69 | 3500 | 86 | 900 | 500 | 100 | Marine | 2538 | 2995 | 1 | 2782 | 2200 | Lower constraint on sea level | Zhang and Peterson, 1984 |
| Watts Lake | 68°36′10″, 78° 13′07″ | | 3 | shells | ZDL70 | 6100 | 108 | 900 | 500 | 100 | Marine | 5745 | 6243 | 1 | 6003 | 5497 | Lower constraint on sea level | Zhang and Peterson, 1984 |
| Watts Lake | 68°36′10″, 78° 13′07″ | | 3 | algae | ZDL71 | 3600 | 95 | 900 | 500 | 100 | Marine | 2707 | 3137 | 1 | 2891 | 2300 | Lower constraint on sea level | Zhang and Peterson, 1984 |
| Triple Lake | 68°31′47″, 78° 14′33″ | | 6 | shells | ZDL78 | 6141 | 90 | 900 | 500 | 100 | Marine | 5866 | 6257 | 1 | 6047 | 5592 | Lower constraint on sea level | Zhang and Peterson, 1984 |

| | | | | | | | | | | | | | | | | | | |
|---|---|---|---|---|---|---|---|---|---|---|---|---|---|---|---|---|---|---|
| Lake Dingle | 68°35′59″, 78° 04′01″ | | 6 | shells | ZDL79 | 5600 | 77 | 900 | 500 | 100 | Marine | 5289 | 5597 | 1 | 5457 | 4851 | Lower constraint on sea level | Zhang and Peterson, 1984 |
| Deep Lake | 68°33′35″, 78° 11′55″ | | 6 | shells | ZDL80 | 6632 | 118 | 900 | 500 | 100 | Marine | 6299 | 6833 | 1 | 6566 | 6067 | Lower constraint on sea level | Zhang and Peterson, 1984 |
| Platcha | 68°30′53″, 78° 28′42″ | | 6 | algae | ZDL81 | 5677 | 94 | 900 | 500 | 100 | Marine | 5307 | 5725 | 1 | 5532 | 4933 | Lower constraint on sea level | Zhang and Peterson, 1984 |
| Watts Lake | 68°36′10″, 78° 13′07″ | | 3.7 | algae | SUA1828 | 4760 | 190 | 900 | 500 | 100 | Marine | 3850 | 4839 | 1 | 4364 | 3694 | Lower constraint on sea level | Adamson and Pickard, 1983 |
| Watts Lake | 68°36′10″, 78° 13′07″ | | 2.4 | sediment | Beta4761 | 6225 | 85 | 900 | 500 | 100 | Marine | 5927 | 6292 | 1 | 6130 | 5649 | Lower constraint on sea level | Adamson and Pickard, 1983 |
| Watts Lake | 68°36′10″, 78° 13′07″ | | 5.5 | shells | SUA2026 | 7590 | 80 | 900 | 500 | 100 | Marine | 7423 | 7711 | 1 | 7569 | 7247 | Lower constraint on sea level | Pickard, 1985 |
| Laternula Lake | 68°38′56″, 78° 58′24″ | | 2 | shells | SUA1411 | 2410 | 90 | 900 | 500 | 100 | Marine | 1284 | 1672 | 1 | 1462 | 1050 | Lower constraint on sea level | Pickard and Adamson, 1983 |
| Death Valley | 68°33′, 78°10′ | | 2.6 | shells | ANU1011 | 4710 | 70 | 900 | 500 | 100 | Marine | 4097 | 4492 | 1 | 4300 | 3666 | Lower constraint on sea level | Adamson and Pickard, 1983 |
| Death Valley | 68°33′, 78°10′ | | 2.6 | shells | SUA1237 | 5340 | 90 | 900 | 500 | 100 | Marine | 4850 | 5333 | 0.996 | 5128 | 4463 | Lower constraint on sea level | Adamson and Pickard, 1983 |
| Calendar Lake | 68°30′45″, 78° 26′52″ | | 1.8 | shells | SUA2030 | 6850 | 160 | 900 | 500 | 100 | Marine | 6450 | 7195 | 1 | 6824 | 6308 | Lower constraint on sea level | Pickard and Seppelt, 1984 |
| Lichen Valley | 68°28′, 78°24′ | | 2 | shells | SUA2027 | 6910 | 150 | 900 | 500 | 100 | Marine | 6546 | 7239 | 1 | 6894 | 6364 | Lower constraint on sea level | Pickard, 1985 |
| Partizan Island | 68°30′17″, 78° 12′05″ | | 3 | shells | Beta4767 | 7370 | 95 | 900 | 500 | 100 | Marine | 7212 | 7557 | 1 | 7381 | 6898 | Lower constraint on sea level | Adamson and Pickard, 1983 |
| *Vestfold Hills, Gardner Island penguin macrofossils* | | | | | | | | | | | | | | | | | | |
| 39,435 | 68°34′40″, 77° 52′14″ | 17 | 32 | Bone | DG-9 | 6110 | 20 | 880 ± 15 | 480 | 100 | Marine | 5932 | 6119 | 1 | 6026 | 5594 | Upper constraint on sea level | Huang et al., 2009a, 2009b |
| 39,436 | 68°34′40″, 77° 52′14″ | 28 | 32 | Bone | DG-18 | 7090 | 25 | 880 ± 15 | 480 | 100 | Marine | 7041 | 7229 | 1 | 7147 | 6650 | Upper constraint on sea level | Huang et al., 2009a, 2009b |
| 39,437 | 68°34′40″, 77° 52′14″ | 42 | 32 | Bone | DG-26 | 7025 | 25 | 880 ± 15 | 480 | 100 | Marine | 6973 | 7150 | 1 | 7066 | 6572 | Upper constraint on sea level | Huang et al., 2009a, 2009b |
| 39,408 | 68°34′40″, 77° 52′14″ | 43 | 32 | Feather | DG-27 | 7335 | 15 | 860 ± 15 | 460 | 100 | Marine | 7326 | 7435 | 1 | 7395 | 6980 | Upper constraint on sea level | Huang et al., 2009a, 2009b |
| 39,409 | 68°34′40″, 77° 52′14″ | 55 | 32 | Feather | DG-30 | 8865 | 20 | 860 ± 15 | 460 | 100 | Marine | 8947 | 9083 | 1 | 9002 | 8463 | Upper constraint on sea level | Huang et al., 2009a, 2009b |
| *Vestfold Hills, Zolotov Island penguin macrofossils* | | | | | | | | | | | | | | | | | | |
| ZOL4–1 | 68°39′29″, 77° 52′09″ | 1 | 7 | Bone | 55,716 | 1340 | 15 | 880 ± 15 | 480 | 100 | Marine | 453 | 518 | 1 | 488 | 83 | Upper constraint on sea level | Huang et al., 2011 |
| ZOL4–8 | 68°39′29″, 77° 52′09″ | 8 | 7 | Bone | 55,717 | 2250 | 15 | 880 ± 15 | 480 | 100 | Marine | 1270 | 1362 | 1 | 1312 | 928 | Upper constraint on sea level | Huang et al., 2011 |
| ZOL4–14 | 68°39′29″, 77° 52′09″ | 14 | 7 | Bone | 55,736 | 2595 | 15 | 880 ± 15 | 480 | 100 | Marine | 1615 | 1780 | 1 | 1699 | 1281 | Upper constraint on sea level | Huang et al., 2011 |
| ZOL4–17 | 68°39′29″, 77° 52′09″ | 17 | 7 | Bone | 55,718 | 3030 | 15 | 880 ± 15 | 480 | 100 | Marine | 2148 | 2297 | 1 | 2229 | 1765 | Upper constraint on sea level | Huang et al., 2011 |
| *Vestfold Hills 'modern' surface samples* | | | | | | | | | | | | | | | | | | |
| Pauk Lake | 68°34′26″, 78° 29′12″ | 0 | | Lake algae | ANU8156 | 112.8 | 2.2 | 0 | 0 | 0 | SH | 62 | 119 | 0.545 | 107 | | Modern reference sample | Zwartz et al., 1998 |
| Lake Bisernoye | 68°31′19″, 78° 30′00″ | 0 | | Lake algae | ANU8164 | 113.4 | 2.5 | 0 | 0 | 0 | SH | 62 | 119 | 0.558 | 106 | | Modern reference sample | Zwartz et al., 1998 |
| Lake Druzhby | 68°35′29″, 78° 16′20″ | 0 | 8 | Lake algae | ANU8169 | 116.9 | 0.9 | 0 | 0 | 0 | SH | 65 | 119 | 0.637 | 101 | | Modern reference sample | Zwartz et al., 1998 |
| 39,410 | 68°34′40″, 77° 52′14″ | 0 | 0 | Feather, modern | DG-33 | 860 | 15 | 860 ± 15 | 460 | 100 | Marine | 7 | 152 | 0.59 | 0 | 0 | Modern reference sample | Huang et al., 2009a, 2009b |
| 39,438 | 68°34′40″, 77° 52′14″ | 0 | 0 | Bone, modern | DG-34 | 880 | 15 | 880 ± 15 | 480 | 100 | Marine | 7 | 152 | 0.59 | 0 | 0 | Modern reference sample | Huang et al., 2009a, 2009b |
| BA07029 | 68°34′40″, 77° 52′14″ | 0 | 0 | Fresh guano, modern | DG-7 | 765 | 45 | 765 ± 45 | 365 | 100 | Marine | 2 | 153 | 0.58 | 0 | 0 | Modern reference sample | Huang et al., 2009a, 2009b |

### 3.2. Rauer Islands

The high resolution diatom analysis of the 1087–900 cm section of sediment core Co1011 (Flag Island depression, 4 m below sea level) included 22 taxa occurring at relative abundances of at least 2.5% in one or more samples (Fig. 2). CONISS cluster analysis and CA of the diatom assemblages identified three significant units spanning a freshwater-to-marine transition (Figs. 2 and 3), that were also consistent with geochemical data (Fig. 4). Dates for unit boundaries were interpolated from the age depth model. Unit I (1081–1075 cm; 11,183–10,669 interpolated cal yr BP) contained freshwater diatoms including *Halamphora veneta*, *Craticula antarctica*, *Stauroforma inermis*, *Nitzschia commutata* and *Navicula gregaria*. *Navicula phyllepta*, a species with broad salinity tolerance and common in East Antarctic lakes (Sabbe et al., 2003), was also present. Unit II (1075–1049 cm; ca. 10,669–9671 interpolated cal yr BP) contained brackish water species common in meromictic brackish lakes in the Vestfold Hills (Roberts and McMinn, 1999), such as *Craspedostauros laevissimus* and *Chamaepinnularia cymatopleura*. Towards the upper part of Unit II, diatoms typical of sea ice including *Fragilariopsis cylindrus*, *Fragilariopsis curta* and *Navicula glaciei* (Cremer et al., 2003) increased in abundance together with *Chaetoceros* resting spores, which are typically associated with open sea water. *N. phyllepta* was still present but fragmented and eroded with often only a raphe remaining (classified as unknown *Navicula* sp. 1 in Fig. 2). In Unit III (1051–1013 cm; 9684–9477 interpolated cal yr BP), *F. cylindrus* became the most abundant species together with *F. curta* and *N. glaciei*, which are all sea ice indicator species. Marine species such as *Thalassiosira gracilis*, *Pseudonitzschia turgiduloides*, *Planothidium engelbrechtii* and *Entomoneis kjellmanii* also appeared above 1051 cm. Total diatom abundance (TDA), driven largely by *F. cylindrus and Chaetoceros* resting spores, was highest between ca. 9615 and 9477 interpolated cal yr BP, coinciding with relatively high total organic carbon (TOC) and total nitrogen (TN) (Fig. 4) immediately after the change to fully marine conditions. The diatom record of a lacustrine-to-marine transition is supported by geochemical data (Fig. 4) with notable decreases in terrigenous inputs (Titanium, Ti) and increases in water content above 1051 cm. This decrease in importance of terrigenous matter, in combination with higher sedimentation rates and increases in diatom abundances and organic matter, illustrate the transition from a small hyper-oligotrophic freshwater lake to a more productive marine system. Spot measurements of the salt content in each zone also showed values increasing from <1% in the freshwater zone to >40% in the marine zone.

The onset of the lacustrine-to-marine transition at Flag Island depression occurs at 1073 cm which falls between age constraints at 1078 cm (10,929 cal yr BP) and 1066 cm (9539 cal yr BP). A linear extrapolation between these dates gives a transition age of 10,349 cal yr BP, and a modelled best fit age of 10,473 interpolated cal yr BP (Table 1). The diatom data and geochemical data indicate that the freshwater to marine transition was complete by 1050 cm which equates to 9678 interpolated cal yr BP, providing a geological constraint on the rising limb of the RSL curve.

### 3.3. Regional summary of geological constraints

Rapid early Holocene RSL rises of c. 12.8 m and c. 3 m are recorded in the Vestfold Hills/Rauer Islands region and the Larsemann Hills, respectively (Fig. 5). Late glacial changes in RSL are not currently constrained in either region, but in the Vestfold Hills rapid RSL rise is recorded between median ages of 9678 cal yr BP, when the Flag Island depression is inundated, and 9411 cal yr BP, when Ace Lake is inundated (note these sites are c. 40 km apart; this is addressed below), with sea level outpacing isostatic rebound at a rate of 48 mm/yr (solid red line, Fig. 5a). A lower rate of 12 mm/yr RSL rise is derived if the timing of the *onset* of the freshwater-to-marine transition at Flag Island is used (modelled best fit age of 10,473 interpolated cal yr BP) rather than the termination (dashed red line, Fig. 5a). In the Larsemann Hills rapid RSL rise is recorded between median ages of 8882 cal yr BP, when Heart Lake is inundated, and 8563 cal yr BP, when Kirisjes Pond is inundated, at a rate of 9.4 mm/yr (Fig. 5b). Prior to this period of rapid RSL rise, RSL at the Larsemann Hills was relatively stable for >1 kyr. In particular, RSL was stable between 9678 and 9411 cal yr BP, during which time RSL rose by c. 12.8 m in the Vestfold Hills region.

An RSL high stand of >8.8 m above sea level (asl) occurs in the Vestfold Hills between 9411 cal yr BP (inundation of Ace Lake) until at least 7564 cal yr BP (interpolated age for the isolation of Anderson Lake is 6765.5 cal yr BP). In the Larsemann Hills an RSL high stand of >8 m asl occurs between 8563 and 7066 cal yr BP (inundation, then isolation of Kirisjes Pond).

Following the RSL high stands the Vestfold Hills geological data suggest an approximately linear decline in RSL through the mid-to-late Holocene (with the exception of the Organic Lake isolation which does not fit the rest of the data). In the Larsemann Hills RSL change is poorly constrained during the mid-Holocene, but RSL fall has been rapid since the isolation of Heart Lake (2703 cal yr BP, 5 m asl) and Pup Lagoon (2092 cal yr BP, 4 m asl).

### 3.4. GIA models

With 20–40 km separation, the RSL history of the Vestfold Hills and Rauer Islands will be different, but predictions are only provided for the Vestfold Hills in the GPM13, BPT14, and ICE-6G_C (VM5a) models. In order to determine whether RSL data from the two sites can be combined to produce a regional RSL curve, model predictions for both locations were generated using the W12 model (Whitehouse et al., 2012b). The results confirm that differences in RSL are likely to be small (model predictions at the two sites differ by <0.2 m during the Holocene), and therefore only predictions for the Vestfold Hills are plotted in Fig. 5. In general, the model predictions provide a reasonable fit to the data as (in some cases, for example W12) they have been tuned to previously published geological constraints.

In the Vestfold Hills all the models predict rapid RSL rise leading into the early Holocene, but at rates slightly lower than the 12–48 mm/yr rise recorded by the isolation basin data between 9678 (or 10,473) and 9411 cal yr BP (Fig. 5a). All four models predict a high stand slightly above the highest isolation basin, at c. 10–12 m asl, with the timing of this high stand occurring within the window constrained by the geological data. The W12 and BPT14 models provide a good fit to the geological data during the mid-to-late Holocene RSL fall, whist the ICE-6G_C (VM5a) and GPM13 models plot slightly below the data-constrained RSL curve.

In the Larsemann Hills there are larger differences between the model predictions, and hence between some of the model predictions and the geological data (Fig. 5b). All the models predict a rapid rise leading into the Holocene, at rates comparable with those recorded by the isolation basin data (9.4 mm/yr). However, in three cases (BPT14, ICE-6G_C (VM5a), GPM13) the timing of the modelled rise through 5–8 m asl predates the geological data by at least 1 kyr, while none of the models resolve the period of stable RSL recorded in the isolation basin data between 10,740 and 8882 cal yr BP. The timing of the Holocene high stand in all models closely fits the age constrained by the geological data, but the height is likely over estimated in all cases, with RSL predicted to have risen between 2 and 14 m above Kirisjes Pond (8 m asl) during the early Holocene. This site was only inundated for c. 1500 yr, and therefore the maximum high stand cannot lie much above the elevation of the lake, which is at a similar elevation to the highest isolation lake in the Vestfold Hills. Only one of the models (W12) predicts a high stand that is at a similar elevation in both the Vestfold and Larsemann Hills. After the RSL maximum, predicted RSL fall at the Larsemann Hills is slightly concave in all models and the change in the rate of RSL fall seen after 2703 cal yr BP is not resolved.

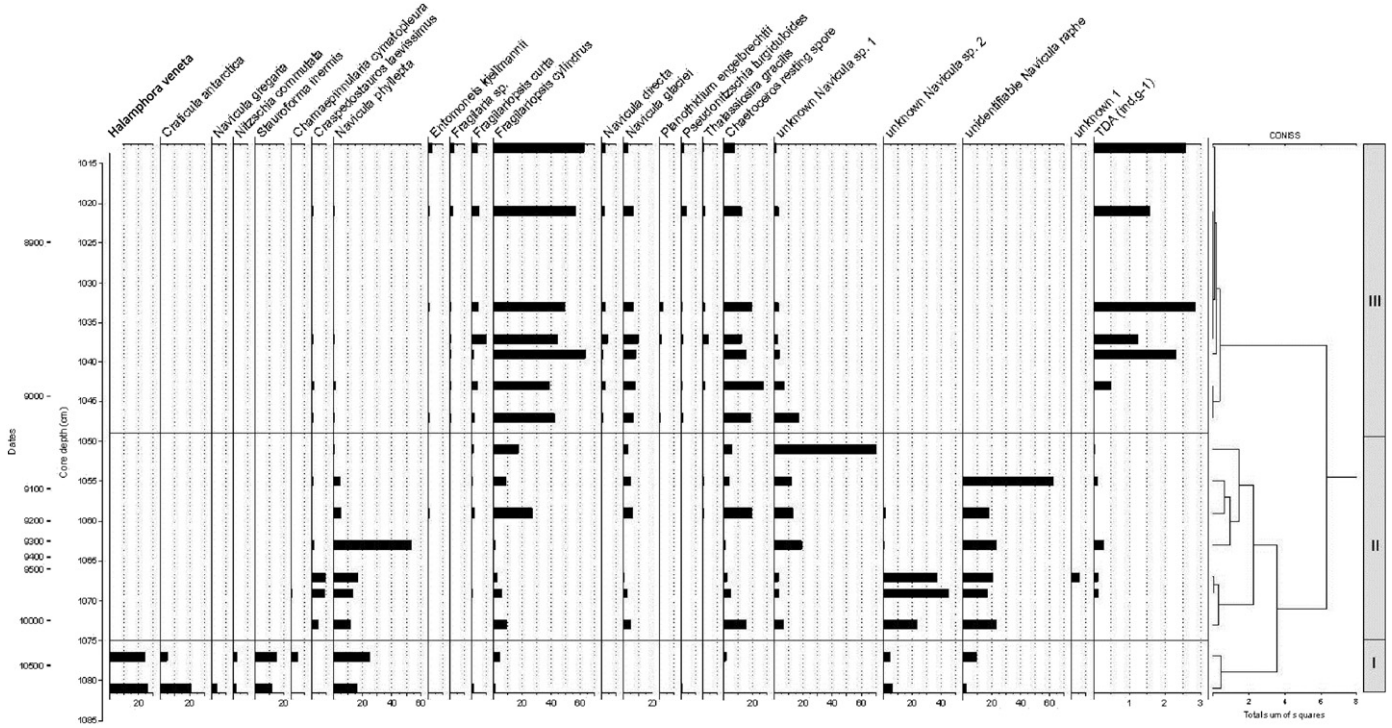


**Fig. 2.** Relative diatom abundances (in percentages) and total diatom abundance (TDA in billions of individuals per gramme sediment) in the 1087–900 cm section of the Co1011 sediment core from the Flag Island depression (Rauer Group). The sediment Units (I–III) are based on a CONISS cluster analysis of relative diatom abundances, confirmed by Correspondence Analysis (CA) (Fig. 3).

## 4. Discussion

This compilation and validation of the RSL constraints in the Prydz Bay region enables an updated evaluation of the regional glacial isostatic and ice sheet history.

### 4.1. Last Glacial Maximum and early deglaciation

Lake sediment records and glacial geomorphology suggest limited ice expansion in the Vestfold Hills at the Last Glacial Maximum (LGM)

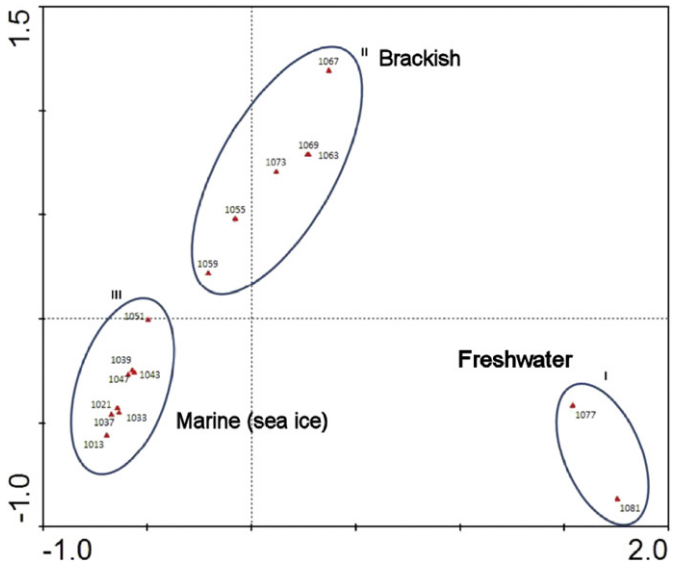


**Fig. 3.** CA showing the CONISS-based subdivision of the investigated Co1011 core section into three units based on log-transformed relative diatom abundances. Unit I, freshwater; Unit II, brackish water; Unit III, marine (sea ice).

(see discussion in Gibson et al., 2009). Cosmogenic $^{10}$Be exposure ages also indicate that the Larsemann Hills were not extensively glaciated at the LGM (Kiernan et al., 2009) and some of the lakes were exposed throughout the last glacial cycle (Hodgson et al., 2005).

Before 10,473 interpolated cal yr BP there are few geological constraints on Holocene sea-level change in the Prydz Bay region (Hodgson et al., 2009). GIA models predict that RSL was below present in the Amery Basin during the LGM, due to the low eustatic sea level. However, the models also indicate that RSL will not have been as low as the global average because the land was depressed due to increased local ice loading, and the sea surface was drawn upwards towards the increased ice mass, both of which act to increase water depths.

Regional ice sheet recession began at about 18,000 cal yr BP in the Lambert/Amery glacial system and at about 14,000 cal yr BP in Mac Robertson Land, it intensified towards ~12,000 cal yr BP and was complete by ~7000 cal yr BP (Mackintosh et al., 2014). In the Vestfold Hills local ice retreat occurred after 12,500 cal yr BP (Gibson et al., 2009) whilst across the Rauer Islands inlets became ice-free prior to 11,200 cal yr BP with glacial minerogenic material continuing to be deposited until ~9200 cal yr BP (Berg et al., 2009, 2010; White et al., 2009). In the Larsemann Hills local ice retreat resulted in the onset of sedimentation in formerly glaciated lakes between c. 15,370 and 12,660 cal yr BP (Verleyen et al., 2005) with most inland lakes being ice-free by 13,500 cal yr BP (Verleyen et al., 2004b).

During deglaciation, solid Earth rebound and perturbations to the geoid in response to local ice mass loss will have offset the sea-level rise that occurred due to the addition of meltwater to the ocean, both by near- and far-field ice sheets. With this in mind, one explanation for the period of relatively stable RSL recorded in the Larsemann Hills between 10,740 and 8882 cal yr BP is that local ice mass loss occurred during this period, with the result that isostatic land uplift was able to keep pace with the ongoing rapid eustatic sea-level rise (Lambeck et al., 2014) for a short period, before the rate of rebound decayed and the global meltwater input once again became the dominant mechanism governing local RSL change. This hypothesis is consistent with

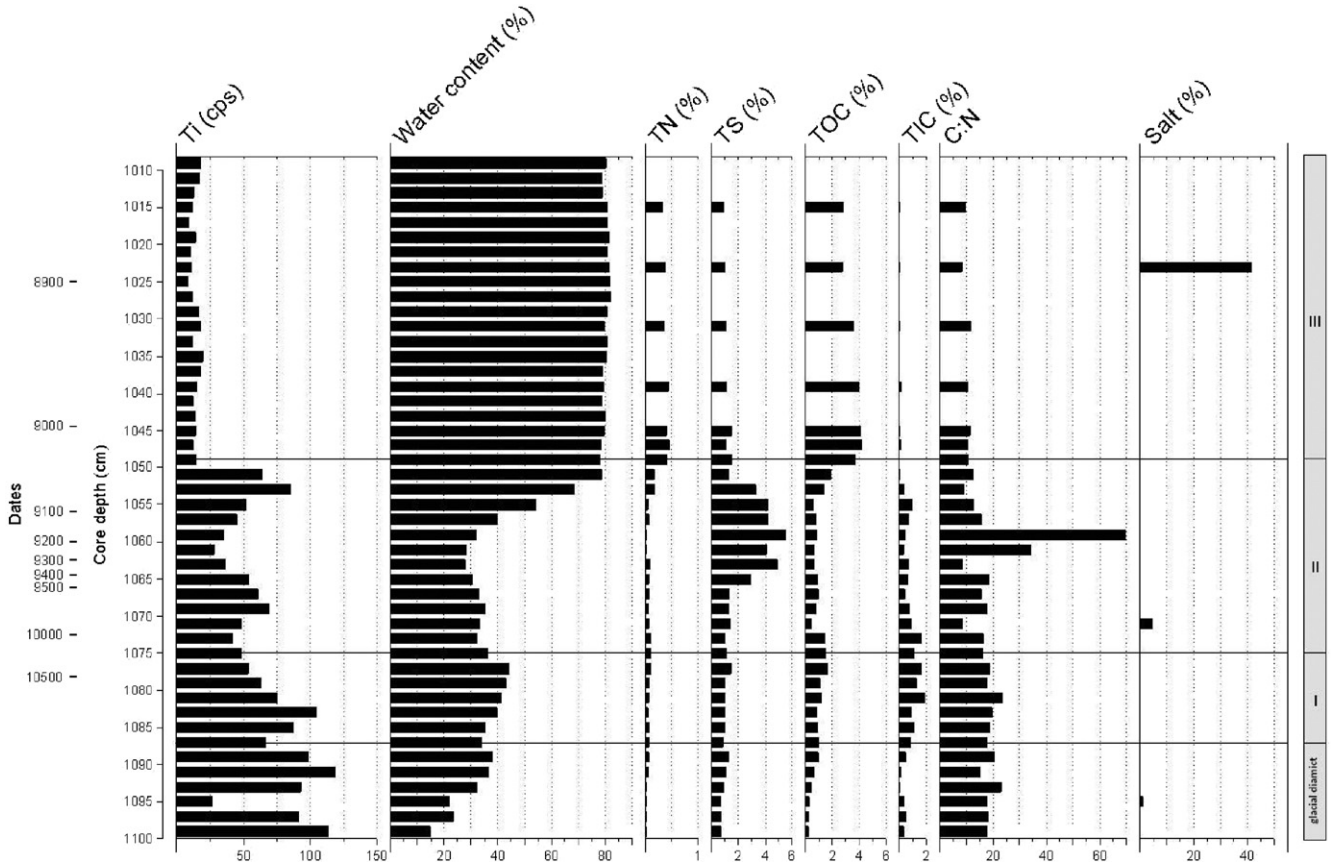


**Fig. 4.** Geochemical data for the 1087–900 cm section of the Co1011 sediment core (Berg et al., 2010), with the three stratigraphic units defined by relative diatom abundances. Ti levels are given as counts per second (cps), other proxies except for C:N are in percentages. The rise in total sulphur (TS) across the freshwater to marine transition is possibly related to bacterial anaerobic respiration resulting from the establishment of meromixis and an anoxic monolimnion. The coincident rapid increase in C:N after ca. 10,473 cal yr BP is consistent with a decrease in benthic cyanobacteria production following marine water incursions into the basin. The establishment of meromixis is likely because the basin was ca. 14.3 m deep before the overlying c. 10.5 m of marine sediment were deposited, which is clearly enough to sustain meromictic conditions as seen in numerous coastal lakes in the nearby Vestfold Hills (Gibson, 1999). The alternative hypothesis that anoxia might be the result of permanent lake-ice cover (Berg et al., 2010) is now considered less likely because (i) relatively high Ti-levels suggest at least seasonal inputs of terrigenous material (although sediment can also reach the water column of perennially frozen lakes to some degree by melting through the ice cover, as illustrated in Jepsen et al. (2010)) (ii) the incursion of marine diatom species is less likely if permanent ice cover was present and (iii) the timing is during the Early Holocene climate optimum in Antarctica (Verleyen et al., 2011) when large areas of the Prydz Bay region were deglaciated (Hodgson et al., 2005).

evidence for the deglaciation of the East Prydz Channel from c. 13,000 cal yr BP, spreading to the Svenner Channel (Barbara et al., 2010a; Domack et al., 1991; Leventer et al., 2006a) and sites beneath the present Amery Ice Shelf by c. 11,000 cal yr BP (Hemer et al., 2007), as reviewed in Mackintosh et al. (2014). Rapid local ice loss during this period, which has been linked to reverse bed slopes in the Amery Depression (O'Brien and Harris, 1996), would result in rapid land uplift and a fall in the height of the geoid, both of which would offset the far-field eustatic signal. The magnitude and timing of the local ice loss could potentially be constrained if isolation basin data were available at a wider range of elevations, including currently-submerged sites, although this approach does require that the sites were ice-free early in the Holocene.

### 4.2. Rapid sea level rises

The rapid RSL rises seen in the Vestfold Hills (9678–9411 cal yr BP, 12.8 m rise at 12–48 mm/yr) and slightly later in the Larsemann Hills (8882–8563 cal yr BP, 3 m rise at 9.4 mm/yr) are considered to be predominantly driven by eustatic sea-level rise, with the differences in rate and timing being due to local isostatic effects. As discussed above, local ice loss can damp the rate of local RSL rise, and hence, conversely, local ice mass gain due to thickening or re-advance has the potential to enhance rates of local RSL rise if the mass gain is sufficient to cause subsidence of the local land surface. However, there is no independent evidence of this in marine geological or lake sediment records (Mackintosh et al., 2014); the only documented advance is the 'Chelnok Advance', a minor lateral expansion of the Sørsdal Glacier which is poorly constrained at no later than 3000–1400 $^{14}$C yr BP (Gore, 1997), <2000 $^{14}$C yr BP (Gore et al., 1996), or 710 corrected yr BP (Fitzsimons and Domack, 1993; Kiernan et al., 2002). The latter estimate was based on a shell macrofossil age of 2010 ± 60 $^{14}$C yr BP which calibrated and corrected for the local marine carbon reservoir (with a nearby modern *Laternula* shell of 950 ± 110 yr BP; SUA 1235) is 755–1263 cal yr BP.

We note that the Larsemann Hills data could be interpreted as recording a sudden pulse of meltwater into the ocean, for example in response to the final drainage of North American Lakes Agassiz and Ojibway prior to 8200 yr BP (Barber et al., 1999). Indeed, this far-field location is likely to have recorded the full eustatic magnitude of this event (Kendall et al., 2008), and the size and duration of the RSL rise at the Larsemann Hills could be used to argue for a prolonged period of freshwater release (Tornqvist and Hijma, 2012), with a total eustatic contribution that lies towards the upper end of proposed estimates (Hijma and Cohen, 2010). However, we caution against using these data to constrain the details of this drainage event for two reasons: First, the period of stable RSL prior to 8882 cal yr BP, which occurred during a period of rapid eustatic sea-level rise, indicates that local RSL changes will clearly be overprinted by local isostatic effects. Secondly, a rapid pulse of RSL rise around 8500 yr BP is not currently detected in the nearby Vestfold Hills, although this may be due to a lack of data at relevant elevations and time periods.

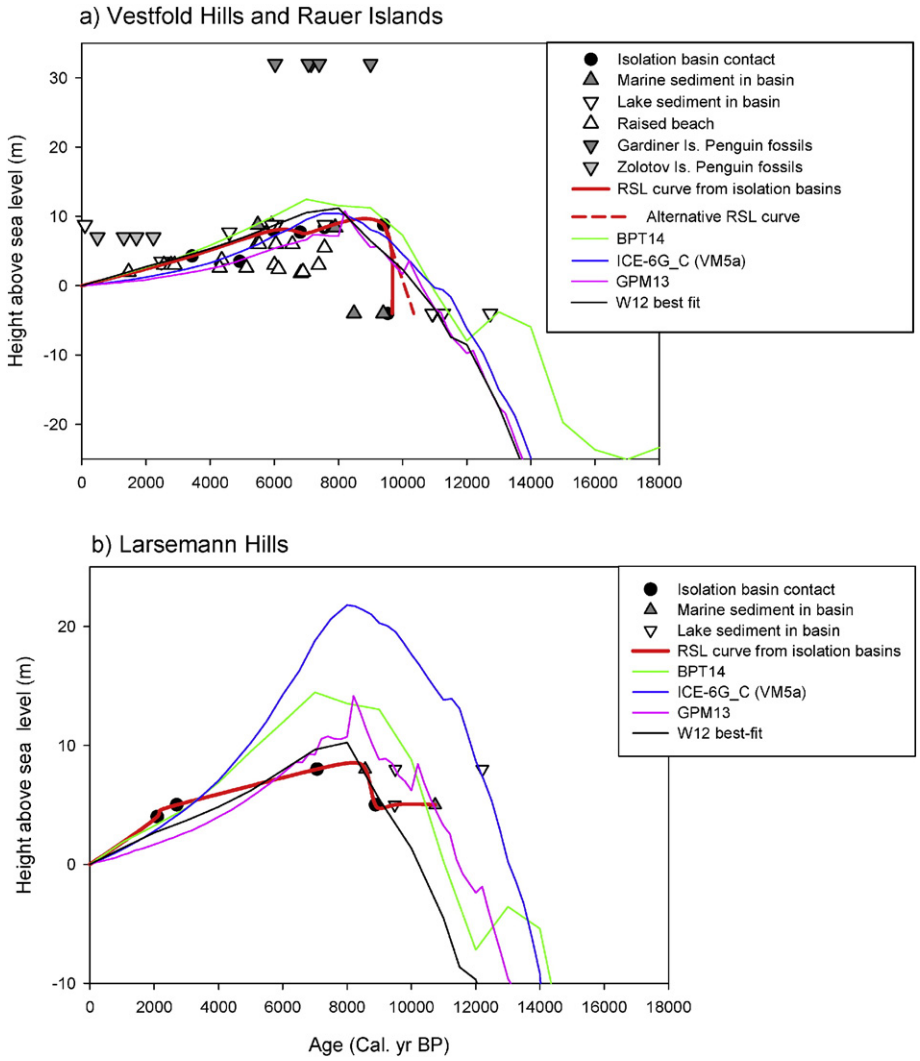


**Fig. 5.** A compilation of RSL data from Prydz Bay plotted together with hypothesised RSL curves (in red) and RSL predictions from a range of GIA models (see key). Vertical errors associated with the RSL curves from isolation basins are discussed in Section 2.1.

### *4.3. RSL high stand*

The timing of the high stand at both the Vestfold and Larsemann Hills is well constrained by geological data, although tighter constraints on the altitude could be obtained from isolation basins at slightly higher elevations. The magnitude of the various modelled high stands for the Vestfold Hills agree very well with the geological data (Fig. 5a), however, simulations for the Larsemann Hills lie 2–14 m above the uppermost geological constraint (Fig. 5b), and there is no published upper sea level constraint for the Rauer Islands (it is likely <11 m asl based on our unpublished observations). The reason for this difference between the regions is that most of the models, with the exception of the W12 model, predict faster Holocene solid Earth rebound at the Larsemann Hills compared with the Vestfold Hills sites, reflecting the proximity of the Larsemann Hills to the assumed ice (un)loading centre in the Amery Basin. The W12 model prescribed limited grounding line advance into Prydz Bay (Whitehouse et al., 2012a), in keeping with the marine record (Barbara et al., 2010b; Domack et al., 1998; Leventer et al., 2006b; Taylor and McMinn, 2002), and hence the volume of regional ice mass change in this model is likely smaller than in some other models.

The inference of a limited regional ice expansion is consistent with evidence that some areas of the Larsemann Hills remained ice-free during the LGM (Hodgson et al., 2001), and the in situ cosmogenic $^{10}$Be exposure dating, radiocarbon determinations, salt and sediment geochemistry, and rock weathering observations (Kiernan et al., 2009) are all consistent with the absence of overriding by a thick ice sheet during the LGM. This supports Gibson et al.'s (2009) hypothesis that the ice that reached the continental shelf margin had its origin in the expansion of large outlet glaciers and ice shelves rather than a general expansion of the regional ice sheet.

The good agreement between the models and geological data in the Vestfold Hills suggests that the models have been successfully tuned to the geological evidence, which indicates minimal ice cover during the LGM. For example, in the north-western region of the Vestfold Hills extensive weathering is consistent with an extended period (possibly 70 000 yr) of subaerial exposure since the last time the area was covered by an erosive, wet-based ice sheet (Gore and Colhoun, 1997). Other areas remained unglaciated, or at least covered by only a thin, non-erosive ice sheet, at the LGM (Fabel et al. 1997; Gibson et al., 2009).

### *4.4. Sea level fall during the Holocene*

In the Vestfold Hills the relatively 'flat' period of RSL between 9411 and 5967 cal yr BP suggests that the final deglacial sea level rise was almost exactly cancelled out by local rebound during this period.

Following the final deglaciation of the Northern Hemisphere ice sheets around 7000 yr BP, eustatic sea levels stabilised, and continued isostatic rebound resulted in a change from RSL rise to RSL fall sometime prior to 7564 and 7066 cal yr BP in the Vestfold Hills and Larsemann Hills, respectively. All the GIA models capture this transition, but they don't capture the acceleration of RSL fall in the Larsemann Hills RSL record from 2703 cal yr BP onwards. This change in rate could be explained if there was a pause in ice retreat, or a small re-advance, sometime during the mid-to-late Holocene, with final deglaciation, and hence rebound, occurring during the last few thousand years. This hypothesis is supported by the late deglaciation of some of the ice proximal lakes around 3470–3687 cal yr BP (Hodgson et al., 2006).

### 4.5. Future research priorities

The interpretation of RSL data from Antarctica will always be hampered by the difficulty of separating contributions from near-field and far-field processes. Near-field RSL data, such as those from the Prydz Bay region, play a crucial role in quantifying local ice mass change, but they may be contaminated by GIA signals associated with poorly constrained regional or continent-scale ice mass change. For example, much better spatial coverage across Antarctica and the sub-Antarctic Islands is required to determine whether the periods of rapid RSL rise recorded in the Larsemann and Vestfold Hills data sets may be linked to meltwater input from the northern hemisphere, or from Antarctica itself.

Large parts of the bed beneath the EAIS are below sea level (Fretwell et al., 2013) and, being vulnerable to ocean-driven melt, may have contributed to sea-level rise during the last interglacial (Mackintosh et al., 2014; Pingree et al., 2011). This makes the study of the rates, timing and forcing of deglaciation in this region a priority. Some constraints on ice-sheet retreat and thickness are available from marine sediment cores, from the submarine geomorphology of the continental shelf, from deglaciation ages of inland mountain ranges (Bentley et al., 2014; Mackintosh et al., 2014) and from RSL data. Overall, however, the coverage of the geological data remains limited.

The scarcity of ice-free sites around the margin of Antarctica means that the approach of directly inferring past ice mass change from local RSL records can only be applied in a few regions. Where RSL data do exist, such as in Prydz Bay, they are mostly limited to the period following the Holocene sea level maximum, and there remain very few constraints on the rising limb of the post-LGM RSL curve. As a result, the largest discrepancies between the GIA model predictions and (the available) geological data occur during the last major deglaciation (Termination 1) and the early Holocene (Fig. 5). This could be addressed by coring former lake basins which now lie below sea level (cf. the Flag Island depression presented in this study). Detailed swath bathymetric surveys of the near-shore marine environment of the Vestfold Hills (O'Brien et al., 2011) (Fig. 6) show clear basin depressions in the submarine topography. During the last glaciation these would have been isolated by a falling sea level and would have accumulated lake sediments; like similar lakes that persisted through the last glacial cycle such as Lake Reid in the Larsemann Hills (Hodgson et al., 2005). Submarine basins are present with sill heights at a range of depths including −6.1 m (Airport Beach), −23.3 m (Davis Anchorage), −32.9 m (Bluff Island) and −46 m (Mule Island) (Fig. 6). Similar surveys of submarine basins have been carried out in the Windmill Islands region and are planned for other sites in East Antarctica. Thus, generating sea-level curves from these submarine depressions must be a priority for refining our understanding of sea-level rise during retreat of the EAIS, and hence improving the GIA correction required by satellite gravity based measurements of contemporary ice mass loss from Antarctica (King et al., 2012). It is possible that some of these depressions may contain both the falling and rising limb of the sea-level curve if any of the basins remained ice-free during the LGM, as is observed in some areas of the Vestfold Hills (Gibson et al., 2009). In the Larsemann Hills, high-elevation sites should be used to get an upper constraint on the maximum level of Early-Holocene RSL, and the post-highstand data set must be considerably expanded if we are to constrain late Holocene

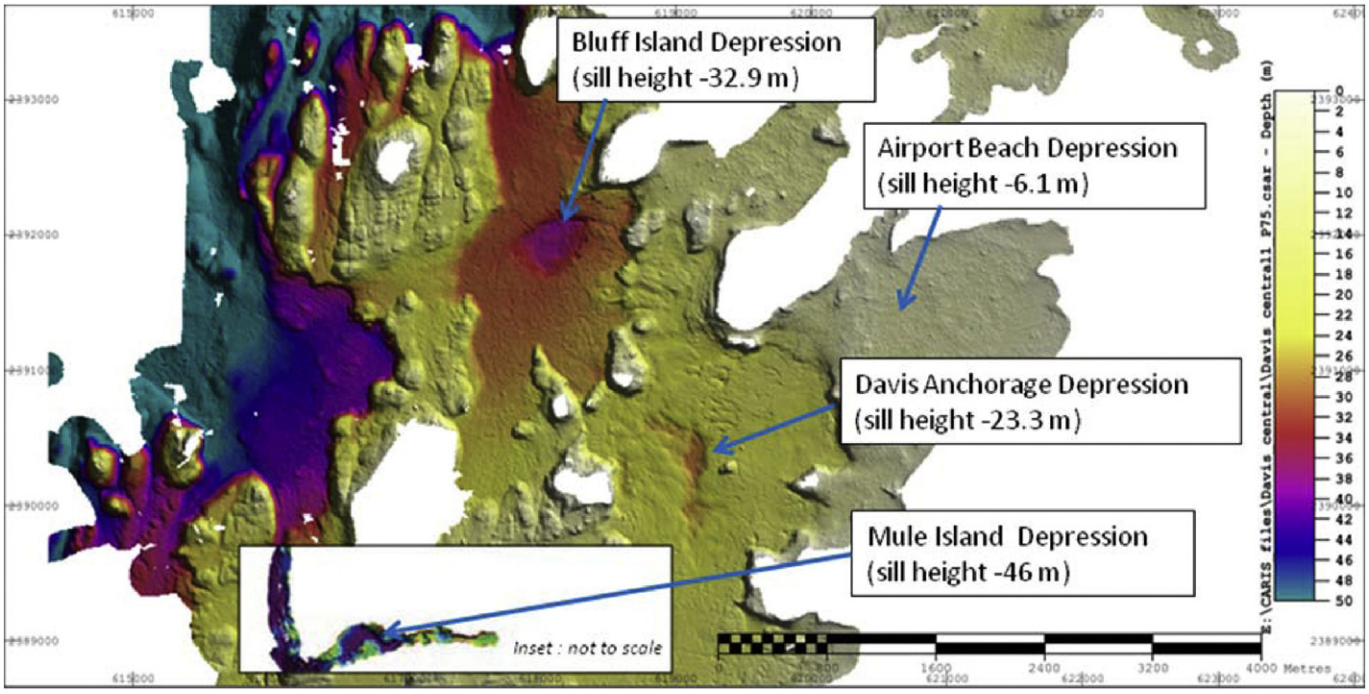


**Fig. 6.** (a) Multibeam swath bathymetry coverage of the Vestfold Hills nearshore zone collected by Geoscience Australia in February to March 2010 showing the submarine basins that could be sampled to provide records of relative sea-level change when sea level was up to 46 m below present. Similar data now exist for the Windmill Islands region (Chris Carson, Geoscience Australia, pers. comm.)

RSL change in this region to the same degree as in the Vestfold Hills. Elsewhere along the East Antarctic margin RSL curves are either in the early stages of development, e.g. at the Bunger Hills (Verkulich et al., 2002), or are absent, e.g. at the Stillwell Hills, and there are little or no near-shore bathymetric survey data.

## 5. Conclusions

RSL data provide a powerful constraint on past regional ice sheet change, and the recalibration and validation of existing and new sea-level constraints from Prydz Bay provides new insights into the deglaciation of a region that drains c. 16% of the EAIS. Key findings in this study are:

(1) There is a lack of geological constraints on sea level prior to 12,000 yr BP with which to constrain GIA models.
(2) We have validated a submerged sea-level data point at Flag Island (Rauer Islands).
(3) We find evidence of rapid sea-level rise in the Prydz Bay region between 9678 and 8563 cal yr BP, predominantly driven by eustatic sea-level rise.
(4) The geological data imply a regional RSL high stand of c. 8 m, which persisted between 9411 cal yr BP and 7564 cal yr BP, and was followed by a period when deglacial sea-level rise was almost exactly cancelled out by local rebound.
(5) We find evidence for two distinct periods of ice retreat in the Larsemann Hills; during the early and late Holocene.
(6) There is a strong case for coring submarine basins offshore of ice-free coastal areas of East Antarctica.

## Acknowledgements

We thank Natalya Gomez, W. Richard Peltier, and Lev Tarasov for providing GIA model results. Data collection in the Rauer Group was funded by the German Research Foundation DFG (grants ME1169/15-1 (Martin Melles) and WA 2109/2-1 (Bernd Wagner) and carried out by the RV Polarstern expedition ANT XXIII/9. Laboratory research was funded by the Natural Environment Research Council UK, and the Belgian Science Policy BELSPO project HOLANT. Ann-Eline Debeer (University of Ghent) helped prepare the diatom samples. Bernd Wagner and Martin Melles led the project that collected sediment cores from the Flag Island depression.

## References

Adamson, D.A., Pickard, J., 1983. Late Quaternary ice movement across the Vestfold Hills, East Antarctica. In: Oliver, R.L., James, P.R., Jago, J.B. (Eds.), Antarctic Earth Science. Aust. Acad. Sci, Canberra ACT, pp. 465–469.
Argus, D.F., Peltier, W.R., Drummond, R., Moore, A.W., 2014. The Antarctica component of postglacial rebound model ICE-6G_C (VM5a) based on GPS positioning, exposure age dating of ice thicknesses, and relative sea level histories. Geophys. J. Int. 197. http://dx.doi.org/10.1093/gji/ggu1140.
Barbara, L., Crosta, X., Masse, G., Ther, O., 2010a. Deglacial environments in eastern Prydz Bay, East Antarctica. Quat. Sci. Rev. 29, 2731–2740.
Barbara, L., Crosta, X., Masse, G., Ther, O., 2010b. Deglacial environments in eastern Prydz Bay, East Antarctica. Quat. Sci. Rev. 29, 2731–2740.
Barber, D.C., Dyke, A., Hillaire-Marcel, C., Jennings, A.E., Andrews, J.T., Kerwin, M.W., Bilodeau, G., McNeely, R., Southon, J., Morehead, M.D., Gagnon, J.M., 1999. Forcing of the cold event of 8,200 years ago by catastrophic drainage of Laurentide lakes. Nature 400, 344–348.
Battarbee, R.W., Kneen, M.J., 1982. The use of electronically counted microspheres in absolute diatom analysis. Limnol. Oceanogr. 27, 184–188.
Bentley, M.J., Ó Cofaigh, C., Anderson, J.B., Conway, H., Davies, B., Graham, A.C., Hillenbrand, C.-D., Hodgson, D.A., Larter, R.D., Mackintosh, A., Verleyen, E., 2014. A community-based geological reconstruction of Antarctic Ice Sheet deglaciation since the Last Glacial Maximum. Quat. Sci. Rev. 100, 1–9.
Berg, S., Wagner, B., White, D.A., Cremer, H., Bennike, O., Melles, M., 2009. New marine core record of Late Pleistocene glaciation history, Rauer Group, East Antarctica. Antarct. Sci. 21, 299–300.
Berg, S., Wagner, B., Cremer, H., Leng, M.J., Melles, M., 2010. Late Quaternary environmental and climate history of Rauer Group, East Antarctica. Palaeogeogr. Palaeoclimatol. Palaeoecol. 297, 201–213.
Bindschadler, R.A., Nowicki, S., Abe-Ouchi, A., Aschwanden, A., Choi, H., Fastook, J., Granzow, G., Greve, R., Gutowski, G., Herzfeld, U., Jackson, C., Johnson, J., Khroulev, C., Levermann, A., Lipscomb, W.H., Martin, M.A., Morlighem, M., Parizek, B.R., Pollard, D., Price, S.F., Ren, D., Saito, F., Sato, T., Seddik, H., Seroussi, H., Takahashi, K., Walker, R., Wang, W.L., 2013. Ice-sheet model sensitivities to environmental forcing and their use in projecting future sea level (the SeaRISE project). J. Glaciol. 59, 195–224.
Bird, M.I., Chivas, A.R., Radnell, C.J., Burton, H.R., 1991. Sedimentological and stable-isotope evolution of lakes in the Vestfold Hills, Antarctica. Palaeogeogr. Palaeoclimatol. Palaeoecol. 84, 109–130.
Blaauw, M., 2010. Methods and code for 'classical' age-modelling of radiocarbon sequences. Quat. Geochronol. 5, 512–518.
Briggs, R., Pollard, D., Tarasov, L., 2013. A glacial systems model configured for large ensemble analysis of Antarctic deglaciation. Cryosphere 7, 1949–1970.
Briggs, R.D., Pollard, D., Tarasov, L., 2014. A data-constrained large ensemble analysis of Antarctic evolution since the Eemian. Quat. Sci. Rev. 103, 91–115.
Church, J.A., Clark, P.U., Cazenave, A., Gregory, J.M., Jevrejeva, S., Levermann, A., Merrifield, M.A., Milne, G.A., Nerem, R.S., Nunn, P.D., Payne, A.J., Pfeffer, W.T., Stammer, D., Unnikrishnan, A.S., 2013. Sea level change. In: Stocker, T.F., Qin, D., Plattner, G.-K., Tignor, M., Allen, S.K., Boschung, J., Nauels, A., Xia, Y., Bex, V., Midgley, P.M. (Eds.), Climate Change 2013: The Physical Science BasisContribution of Working Group I to the Fifth Assessment Report of the Intergovernmental Panel on Climate Change. Cambridge University Press, Cambridge, United Kingdom and New York, NY, USA, pp. 1137–1216.
Coolen, M.J.L., Muyzer, G., Rijpstra, W.I.C., Schouten, S., Volkman, J.K., Sinninghe Damsté, J.S., 2004. Combined DNA and lipid analyses of sediments reveal changes in Holocene haptophyte and diatom populations in an Antarctic lake. Earth Planet. Sci. Lett. 223, 225–239.
Cremer, H., Roberts, D., McMinn, A., Gore, D., Melles, M., 2003. The Holocene diatom flora of marine bays in the Windmill Islands, East Antarctica. Bot. Mar. 46, 82–106.
Damm, V., 2007. A subglacial topographic model of the southern drainage area of the Lambert Glacier/Amery Ice Shelf System. Results of an airborne ice thickness survey south of the Prince Charles Mountains. Terra Antarct. 14, 85–94.
Domack, E.W., Jull, A.J.T., Nakao, S., 1991. Advance of east Antarctic outlet glaciers during the hypsithermal — implications for the volume state of the Antarctic Ice-Sheet under global warming. Geology 19, 1059–1062.
Domack, E., O'Brien, P., Harris, P., Taylor, F., Quilty, P.G., De Santis, L., Raker, B., 1998. Late Quaternary sediment facies in Prydz Bay, East Antarctica and their relationship to glacial advance onto the continental shelf. Antarct. Sci. 10, 236–246.
Fabel, D., Stone, J., Fifield, L.K., Cresswell, R.G., 1997. Deglaciation of the Vestfold Hills, East Antarctica: preliminary evidence from exposure dating of three subglacial erratics. In: Ricci, C.A. (Ed.), The Antarctic Region: Geological Evolution and Processes. Proceedings 7th International Symposium on Antarctic Earth Science, Siena, 1995, pp. 829–834.
Farrell, W.E., Clark, J.A., 1976. On postglacial sea level. Geophys. J. R. Astron. Soc. 46, 647–667.
Fitzsimons, S.J., Domack, E.W., 1993. Evidence for early Holocene deglaciation of the Vestfold Hills, east Antarctica. Polar Rec. 29, 237–240.
Fretwell, P., Pritchard, H.D., Vaughan, D.G., Bamber, J.L., Barrand, N.E., Bell, R., Bianchi, C., Bingham, R.G., Blankenship, D.D., Casassa, G., Catania, G., Callens, D., Conway, H., Cook, A.J., Corr, H.F.J., Damaske, D., Damm, V., Ferraccioli, F., Forsberg, R., Fujita, S., Gim, Y., Gogineni, P., Griggs, J.A., Hindmarsh, R.C.A., Holmlund, P., Holt, J.W., Jacobel, R.W., Jenkins, A., Jokat, W., Jordan, T., King, E.C., Kohler, J., Krabill, W., Riger-Kusk, M., Langley, K.A., Leitchenkov, G., Leuschen, C., Luyendyk, B.P., Matsuoka, K., Mouginot, J., Nitsche, F.O., Nogi, Y., Nost, O.A., Popov, S.V., Rignot, E., Rippin, D.M., Rivera, A., Roberts, J., Ross, N., Siegert, M.J., Smith, A.M., Steinhage, D., Studinger, M., Sun, B., Tinto, B.K., Welch, B.C., Wilson, D., Young, D.A., Xiangbin, C., Zirizzotti, A., 2013. Bedmap2: improved ice bed, surface and thickness datasets for Antarctica. Cryosphere 7, 375–393.
Gibson, J.A.E., 1999. The meromictic lakes and stratified marine basins of the Vestfold Hills, East Antarctica. Antarct. Sci. 11, 175–192.
Gibson, J.A.E., Paterson, K.S., White, C.A., Swadling, K.M., 2009. Evidence for the continued existence of Abraxas Lake, Vestfold Hills, East Antarctica during the Last Glacial Maximum. Antarct. Sci. 21, 269–278.
Gomez, N., Pollard, D., Mitrovica, J.X., 2013. A 3-D coupled ice sheet-sea level model applied to Antarctica through the last 40 ky. Earth Planet. Sci. Lett. 384, 88–99.
Gore, D.B., 1997. Last glaciation of Vestfold Hills: extension of east Antarctic ice sheet or lateral expansion of Sørsdal Glacier. Polar Rec. 33, 5–12.
Gore, D.B., Colhoun, E.A., 1997. Regional contrasts in weathering and glacial sediments: long-term subaerial exposure of Vestfold Hills. In: Ricci, C.A. (Ed.), The Antarctic Region: Geological Evolution and Processes. Proceedings 7th International Symposium on Antarctic Earth Science, Siena, 1995, pp. 835–839.
Gore, D.B., Pickard, J., Baird, A.S., Webb, J.A., 1996. Glacial Crooked Lake, Vestfold Hills, East Antarctica. Polar Rec. 32, 19–24.
Grimm, E.C., 1987. CONISS: a FORTRAN 77 program for stratigraphically constrained cluster analysis by the method of incremental sum of squares. Comput. Geosci. 13, 13–35.
Grimm, E.C., 1991. TILIA and TILIAGRAPH. Illinois State Museum, Springfield.
Grimm, E.C., 2004. TGView version 2.0.2. Illinois State Museum, Springfield.
Hall, B.L., Henderson, G.M., 2001. Use of uranium-thorium dating to determine past $^{14}C$ reservoir effects in lakes: examples from Antarctica. Earth Planet. Sci. Lett. 193, 565–577.
Hemer, M.A., Post, A.L., O'Brien, P.E., Craven, M., Truswell, E.M., Roberts, D., Harris, P.T., 2007. Sedimentological signatures of the sub-Amery Ice Shelf circulation. Antarct. Sci. 19, 497–506.

Hijma, M.P., Cohen, K.M., 2010. Timing and magnitude of the sea-level jump preluding the 8200 yr event. Geology 38, 275–278.
Hodgson, D.A., Noon, P.E., Vyverman, W., Bryant, C.L., Gore, D.B., Appleby, P., Gilmour, M., Verleyen, E., Sabbe, K., Jones, V.J., Ellis-Evans, J.C., Wood, P.B., 2001. Were the Larsemann Hills ice-free through the Last Glacial Maximum? Antarct. Sci. 13, 440–454.
Hodgson, D.A., Verleyen, E., Sabbe, K., Squier, A.H., Keely, B.J., Leng, M.J., Saunders, K.M., Vyverman, W., 2005. Late quaternary climate-driven environmental change in the Larsemann Hills, East Antarctica, multi-proxy evidence from a lake sediment core. Quat. Res. 64, 83–99.
Hodgson, D.A., Verleyen, E., Squier, A.H., Sabbe, K., Keely, B.J., Saunders, K.M., Vyverman, W., 2006. Interglacial environments of coastal east Antarctica: comparison of MIS 1 (Holocene) and MIS 5e (Last Interglacial) lake-sediment records. Quat. Sci. Rev. 25, 179–197.
Hodgson, D.A., Verleyen, E., Vyverman, W., Sabbe, K., Leng, M.J., Pickering, M., Keely, B.J., 2009. A geological constraint on relative sea level in Marine Isotope Stage 3 in the Larsemann Hills, Lambert Glacier region, East Antarctica (31 366 - 33 228 cal yr BP). Quat. Sci. Rev. 28, 2689–2696.
Hogg, A.G., Hua, Q., Blackwell, P.G., Niu, M., Buck, C.E., Guilderson, T.P., Heaton, T.J., Palmer, J.G., Reimer, P.J., Reimer, R.W., Turney, C.S.M., Zimmerman, S.R.H., 2013. SHCal13 Southern Hemisphere Calibration, 0-50,000 Years cal BP. Radiocarbon 55 (4).
Huang, T., Sun, L., Wang, Y., Liu, X., Zhu, R., 2009a. Penguin population dynamics for the past 8500 years at Gardner Island, Vestfold Hills. Antarct. Sci. 21, 571–578.
Huang, T., Sun, L., Wang, Y., Zhu, R., 2009b. Penguin occupation in the Vestfold Hills. Antarct. Sci. 21, 131–134.
Huang, T., Sun, L., Wang, Y., Kong, D., 2011. Late Holocene Adélie penguin occupation history and population dynamics at Zolotov Island, Vestfold Hills. J. Paleolimnol. 45, 273–285.
Jepsen, S.M., Adams, E.E., Priscu, J.C., 2010. Sediment melt-migration dynamics in Perennial Antarctic Lake Ice. Arct. Antarct. Alp. Res. 42, 57–66.
Kendall, R.A., Mitrovica, J.X., Milne, G.A., Tornqvist, T.E., Li, Y.X., 2008. The sea-level fingerprint of the 8.2 ka climate event. Geology 36, 423–426.
Kiernan, K., McConnell, A., Colhoun, E.A., Lawson, E., 2002. Radiocarbon dating of mumiyo from the Vestfold Hills, East Antarctica. Pap. Proc. R. Soc. Tasmania 136, 141–144.
Kiernan, K., Gore, D.B., Fink, D., White, D.A., McConnell, A., Sigurdsson, I.A., 2009. Deglaciation and weathering of Larsemann Hills, East Antarctica. Antarct. Sci. 21, 373–382.
King, M.A., Bingham, R.J., Moore, P., Whitehouse, P.L., Bentley, M.J., Milne, G.A., 2012. Lower satellite-gravimetry estimates of Antarctic sea-level contribution. Nature 491, 586–589. http://dx.doi.org/510.1038/nature11621.
Lambeck, K., Rouby, H., Purcell, A., Sun, Y.Y., Sambridge, M., 2014. Sea level and global ice volumes from the Last Glacial Maximum to the Holocene. Proc. Natl. Acad. Sci. U. S. A. 111, 15296–15303.
Leventer, A., Domack, E., Dunbar, R., Pike, J., Stickley, C., Maddison, E., Brachfeld, S., Manley, P., McClennen, C., 2006a. Marine sediment record from the East Antarctic margin reveals dynamics of ice sheet recession. GSA Today 16, 4–10.
Leventer, A., Domack, E., Dunbar, R., Pike, J., Stickley, C., Maddison, E., Brachfeld, S., Manley, P., McClennen, C., 2006b. Marine sediment record from the East Antarctic margin reveals dynamics of ice sheet recession. GSA Today 16, 4–10.
Mackintosh, A.N., Verleyen, E., O'Brien, P.E., White, D., McKay, R., Gore, D.B., Dunbar, R., Fink, D., Jones, S., Post, A.L., Miura, H., Leventer, A., Goodwin, I., Lilly, K., Crosta, X., Golledge, N., Wagner, B., Berg, S., van Ommen, T., Zwartz, D., Hodgson, D.A., Roberts, S.J., Vyverman, W., Masse, G., 2014. Retreat history of the East Antarctic Ice Sheet since the Last Glacial Maximum. Quat. Sci. Rev. 100, 10–30.
O'Brien, P.E., Harris, P.T., 1996. Patterns of glacial erosion and deposition in Prydz Bay and the past behaviour of the Lambert Glacier. Pap. Proc. R. Soc. Tasmania 130 (2), 79–85.
O'Brien, P.E., Atkinson, I., Bowden, R., Forrest, D., Paddison, J., Swanson, S., 2011. Coastal Seabed Mapping Survey, Vestfold Hills, Antarctica, February–March 2010 (AAS 2201) – Post Survey Report, Record 2010/47, GeoCat # 71368 (34 pp.).
Peltier, W.R., 2004. Global glacial isostasy and the surface of the ice-age Earth: The ICE-5G (VM2) model and GRACE. Annu. Rev. Earth Planet. Sci. 32, 111–149.
Peltier, W.R., Drummond, R., 2008. Rheological stratification of the lithosphere: a direct inference based upon the geodetically observed pattern of the glacial isostatic adjustment of the North American continent. Geophys. Res. Lett. 35.
Peltier, W.R., Argus, D.F., Drummond, R., 2015. Space geodesy constrains ice age terminal deglaciation: the global ICE-6G_C (VM5a) model. J. Geophys. Res. Solid Earth Planets 120, 450–487.
Pickard, J., 1985. The Holocene fossil marine macrofauna of the Vestfold Hills, East Antarctica. Boreas 14, 189–202.
Pickard, J., Adamson, D.A., 1983. Holocene marine deposits and ice retreat, Vestfold Hills, Antarctica 7 +/−2 ka to present. In: Chappell, J.M.A., Grindrod, A. (Eds.), First CLIMANZ Conference,. Dep. Biogeogr. Geomorphol., Aust. Natl. Univ., Canberra, A.C.T, p. 110.
Pickard, J., Seppelt, R.D., 1984. Holocene occurrence of the moss *Bryum algens* card in the Vestfold Hills, Antarctica. J. Bryol. 13, 209–217.
Pingree, K., Lurie, M., Hughes, T., 2011. Is the East Antarctic ice sheet stable? Quat. Res. 75, 417–429.
Reimer, P.J., Bard, E., Bayliss, A., Beck, J.W., Blackwell, P.G., Bronk Ramsey, C., Grootes, P.M., Guilderson, T.P., Haflidason, H., Hajdas, I., HattŽ, C., Heaton, T.J., Hoffmann, D.L., Hogg, A.G., Hughen, K.A., Kaiser, K.F., Kromer, B., Manning, S.W., Niu, M., Reimer, R.W., Richards, D.A., Scott, E.M., Southon, J.R., Staff, R.A., Turney, C.S.M., van der Plicht, J., 2013. IntCal13 and Marine13 Radiocarbon Age Calibration Curves 0-50,000 Years cal BP. Radiocarbon 55 (4).
Roberts, D., McMinn, A., 1999. Diatoms of the saline lakes of the Vestfold Hills, Antarctica. Bibl. Diatomol. 44, 83.
Roberts, S.J., Hodgson, D.A., Sterken, M., Whitehouse, P.L., Verleyen, E., Vyverman, W., Sabbe, K., Balbo, A., Bentley, M.J., Moreton, S.G., 2011. Geological constraints on glacio-isostatic adjustment models of relative sea-level change during deglaciation of Prince Gustav Channel, Antarctic Peninsula. Quat. Sci. Rev. 30, 3603–3617.
Sabbe, K., Verleyen, E., Hodgson, D.A., Vyverman, W., 2003. Benthic diatom flora of freshwater and saline lakes in the Larsemann Hills and Rauer Islands, East Antarctica. Antarct. Sci. 15, 227–248.
Taylor, F., McMinn, A., 2002. Late Quaternary diatom assemblages from Prydz Bay, Eastern Antarctica. Quat. Res. 57, 151–161.
ter Braak, C.J.F., Smilauer, P., 2002. CANOCO reference manual and CanoDraw for windows user's guide: software for canonical community ordination (version 4.5). Microcomputer Power, Ithaca, NY, USA.
Tornqvist, T.E., Hijma, M.P., 2012. Links between early Holocene ice-sheet decay, sea-level rise and abrupt climate change. Nat. Geosci. 5, 601–606.
Verkulich, S.R., Melles, M., Pushina, Z.V., Hubberten, H.-W., 2002. Holocene environmental changes and development of Figurnoye Lake in the southern Bunger Hills, East Antarctica. J. Paleolimnol. 28, 253–267.
Verleyen, E., Hodgson, D.A., Vyverman, W., Roberts, D., McMinn, A., Vanhoutte, K., Sabbe, K., 2003. Modelling diatom responses to climate induced fluctuations in the moisture balance in continental Antarctic lakes. J. Paleolimnol. 30, 195–215.
Verleyen, E., Hodgson, D.A., Sabbe, K., Vanhoutte, K., Vyverman, W., 2004a. Coastal oceanographic conditions in the Prydz Bay region (East Antarctica) during the Holocene recorded in an isolation basin. The Holocene 14, 246–257.
Verleyen, E., Hodgson, D.A., Sabbe, K., Vyverman, W., 2004b. Late Quaternary deglaciation and climate history of the Larsemann Hills (East Antarctica). J. Quat. Sci. 19, 361–375.
Verleyen, E., Hodgson, D.A., Milne, G.A., Sabbe, K., Vyverman, W., 2005. Relative sea level history from the Lambert Glacier Region (East Antarctica) and its relation to deglaciation and Holocene glacier re-advance. Quat. Res. 63, 45–52.
Verleyen, E., Hodgson, D.A., Sabbe, K., Cremer, H., Emslie, S.D., Gibson, J., Hall, B., Imura, S., Kudoh, S., Marshall, G.J., McMinn, A., Melles, M., Newman, L., Roberts, D., Roberts, S.J., Singh, S.M., Sterken, M., Tavernier, I., Verkulich, S., Van de Vyver, E., Van Nieuwenhuyze, W., Wagner, B., Vyverman, W., 2011. Post-glacial regional climate variability along the East Antarctic coastal margin — evidence from shallow marine and coastal terrestrial records. Earth-Sci. Rev. 104, 199–212.
Wahr, J., Wingham, D., Bentley, C., 2000. A method of combining ICESat and GRACE satellite data to constrain Antarctic mass balance. J. Geophys. Res. 105, 16,279–216,294.
Watcham, E.P., Bentley, M.J., Hodgson, D.A., Roberts, S.J., Fretwell, P.T., Lloyd, J.M., Larter, R.D., Whitehouse, P.L., Leng, M.J., Monien, P., Moreton, S.G., 2011. A new relative sea level curve for the South Shetland Islands, Antarctica. Quat. Sci. Rev. 30, 3152–3170.
White, D.A., Bennike, O., Berg, S., Harley, S.L., Fink, D., Kiernan, K., McConnell, A., Wagner, B., 2009. Geomorphology and glacial history of Rauer Group, East Antarctica. Quat. Res. 72, 80–90.
Whitehouse, P.L., Bentley, M.J., Le Brocq, A.M., 2012a. A deglacial model for Antarctica: geological constraints and glaciological modelling as a basis for a new model of Antarctic glacial isostatic adjustment. Quat. Sci. Rev. 32, 1–24.
Whitehouse, P.L., Bentley, M.J., Milne, G.A., King, M.A., Thomas, I.D., 2012b. A new glacial isostatic adjustment model for Antarctica: calibrating the deglacial model using observations of relative sea-level and present-day uplift rates. Geophys. J. Int. 190, 1464–1482.
Zhang, Q., Peterson, J.A., 1984. A geomorphology and Late Quaternary geology of the Vestfold Hills, Antarctica. Australian Government Publishing Service, Canberra.
Zwartz, D., Bird, M., Stone, J., Lambeck, K., 1998. Holocene sea-level change and ice-sheet history in the Vestfold Hills, East Antarctica. Earth Planet. Sci. Lett. 155, 131–145.